Continuation of Research in Seismic Techniques for Characterizing Levees: Las Cruces, NM Component

Richard D. Miller
Julian Ivanov
Shelby L. Walters

Kansas Geological Survey
1930 Constant Avenue
University of Kansas
Lawrence, KS 66047

Final Report to

Joseph B. Dunbar
U.S. Army Corps of Engineers – WES
3909 Halls Ferry Road
Vicksburg, MS 39180

Open-file Report No. 2007-17 June 2007

Continuation of Research in Seismic Techniques for Characterizing Levees: Las Cruces, NM Component

Richard D. Miller
Julian Ivanov
Shelby L. Walters

Kansas Geological Survey
1930 Constant Avenue
University of Kansas
Lawrence, Kansas 66047

Final Report to

Joseph B. Dunbar
U.S. Army Corps of Engineers – WES
3909 Halls Ferry Road
Vicksburg, MS 39180

KGS Open-file Report 2007-17

June 2007

TABLE OF CONTENTS

GLOSSARY OF ACRONYMS

A/D	analog to digital
AGC	automatic gain control
CDP	common depth point (reflection seismic)
CMP	common mid point (reflection seismic), similar to CDP
DGPS	differential global positioning system
DC	direct current
EM	electromagnetic
FDSE	filtering dispersive seismic event
GPS	global positioning system
IBWC	International Boundary and Water Commission
JARS	joint analysis of refractions and surface waves
KGS	Kansas Geological Survey
MASW	multi-channel analysis of surface waves
MPC	Mobile Processing Center
NMO	normal move out (reflection seismic)
Q	quality factor (measure of seismic attenuation)
QA	quality assurance
QC	quality control
RMS	root mean square
SASW	spectral analysis of surface waves
SEG2	Society of Exploration Geophysics seismic data format
SEGY	Society of Exploration Geophysics seismic data format
Vp	compressional-wave velocity
Vs	shear-wave velocity

Continuation of Research in Seismic Techniques for Characterizing Levees: Las Cruces, NM Component

EXECUTIVE SUMMARY

Seismic research detailed in this report is part of an exhaustive and comprehensive study by the U.S. Army Corps of Engineers formulated to evaluate the integrity of levees along the Rio Grande River. This particular part of that applied research project focused on adapting a variety of seismic methods to characterize the physical condition of and changes in levee cores and foundations that might be expected as a result of prolonged flood river levels at or near the design limits of the levees. Most levees along the Rio Grande River were originally constructed in the 1930s and 1940s as part of the International Boundary and Water Commission (IBWC) program in south New Mexico. These series of investigations (Weslaco, Texas, and Las Cruces, New Mexico) are the first explicitly designed to evaluate the sensitivity of seismic methods to detect water infiltration and any changes in core strength during a mock flood event at a real levee site.

Seismic methods have proven marginally successful at identifying anomalies in levees previously on a few occasions. Most of these studies have focused on direct wave analysis, targeting areas with reduced seismic velocities. Lower seismic velocities are usually indicative of less strength or softer materials. Therefore, anomalously low velocities for a particular levee could be an early indicator of failure potential. Based on currently available scientific literature, seismic testing at each of the five sites in Texas and three in New Mexico as part of this IBWC research program has been more extensive than at any previous earthen structure study. The testing included compressional first-arrival analysis (classic refraction, turning-ray tomography), multichannel surface-wave analysis, and vibration harmonics analysis. Tests were conducted on the levee crest with expanded studies at sites identified as good candidates for ponding experiments.

Three sites with different surface characteristics along a mile-plus-long stretch of levee west of Las Cruces were selected and subjected to continuous split-spoon sampling, surface electrical and EM interrogation, and a variety of seismic imaging. From these initial studies and surface evaluations a single site was selected that possessed seismic characteristics suggested to represent the structurally weakest of the sites, which, compounded with rodent burrows evident in the levee shell, makes it the best choice. Preliminary seismic investigations indicated the selected ponding site possessed slightly lower shear velocities and distinctly interpretable fundamental-mode surface-wave energy within the higher frequency portion of the spectra. This site was selected for the ponding experiment based on several characteristics indicative of structural weakness and therefore the greatest failure potential during a simulated full-board event.

A simulated flood event was orchestrated coincident with a series of near-surface geophysical surveys. These geophysical surveys were time-lapse with the hope that both absolute and relative changes and measurements would be consistent with structural and/or material properties indicative of levee strength. Ideally these changes could be directly related to levee fitness and establish areas susceptible to levee breech. In general, both compressional- and shear-wave velocity estimates for this fine-sand levee near Las Cruces were indicative of increased pore fluid resulting from the increased head associated with the pond. Even though no failure occurred, the observed increased Vp and decreased Vs values, and thus decreased levee strength, could eventually result in levee failure.

Two trips to the levee sites resulted in seismic data sets with uniquely different characteristics. Comparing the Vp and Vs estimates between the two trips shows that, at the time of trip 2,

there is a general decrease of Vs and at least 15% increase of Vp within the levee (top 10 ft) compared to trip 1. A Vp velocity increase between 15 and 20% is evident for most of the top 10 ft, with the exception of the 2110-2160 ft offset range, where the velocity decrease is more than 40%. It is hypothesized that Vp velocity increase is due to higher moisture content in the fine-sand levee shell, a suggestion that is consistent with the rainy period experienced in this area after the first trip.

The Vp/Vs ratio (Poisson's ratio) is higher during trip 2 in comparison to trip 1. High Vp/Vs ratio can produce larger amplitude higher modes and weaker fundamental mode as observed during the second trip. This observation is important to the overall understanding and significance of results from MASW surveys. It is relatively easy to estimate the fundamental mode of the surface wave from data acquired during the first trip, while it is very challenging to evaluate it during the second trip.

The baseline compressional-wave survey during the ponding experiment revealed a high-velocity Vp anomaly between locations 2120 and 2160 ft, an area characterized by a large number of animal burrows. This anomaly extended to 10 ft of depth near the start of the flooding experiment and after the first 4 hours could still only be observed within the very top 3-4 ft of the levee. Refraction-tomography Vp results for the rest of the line suggest compressional-wave velocity does not appear sensitive to any changes in seismic characteristics of affected levee material that can be attributed to the ponding. It is also possible that, once saturated, the clay particles within levee surface or skin sealed and resisted saturation, and therefore no material changes actually took place within the principal imaged zone of the levee.

A baseline MASW survey was designed to establish an initial 2-D Vs section and to be used as a reference for subsequent time-lapse surveys. Two anomalous high-velocity zones can be observed within the levee body at a depth of about 6 ft between locations 2095 and 2103 ft, and 2145 and 2165 ft. At time slices 2 and 3, representing 4 and 8 hours after the start of the water fill, the shear-wave properties change and the high-velocity anomalies begin to diminish. As the flooding simulation continues at time slices 3, 4, and 5, the Vs values within the levee continue to decrease to about 10-15% of their original values. At the same time, a new low-velocity zone begins to form between locations 2098 and 2110 ft at depths greater than 11 ft below the crown of the levee.

This trend continues during time slices 6 and 7, and by time slices 8 and 9 the low-velocity anomaly is well established and clearly represents a change in the seismic characteristics of the levee and its foundation. Most likely this anomaly relates to ground water movement under the levee. Such water movement could result in piping making this section of levee susceptible to reduced strength and therefore performance that might not meet design specifications. These anomalies could be catalysts for seepage and therefore threaten levee core integrity, indicative of zones susceptible to failure in extreme cases where the levee is exposed to prolonged high-water conditions. Detection of such anomalies meets one of the objectives of the survey, which is to detect old streambeds running under the levees that could provide conduits for increased groundwater flow, thereby indicative of weak spots more prone to failure during flooding.

Time-lapse shear-wave profiles calculated from surface-wave energy using the MASW method appear to have changed with increased water depth during the ponding experiment. We assumed these seismic changes are in response to increased saturation below the levee as water infiltrated the foundation during the flood simulation. No noticeable changes occurred in the compressional-wave properties within the levee except for a small volume speculated to be compromised by animal burrows. Vs was the measured material property most significantly affected from increased saturation driven by the hydraulic head provided by the water in the pond.

INTRODUCTION

In support of the U.S. Army Corps of Engineers' strong commitment to dam and levee safety, new and/or adaptations of existing technologies need to be identified and evaluated at sites with both physical characteristics conducive to those technologies and a history of substandard dam or levee performance. Models used to predict dam or levee performance levels during earthquakes and floods are only as realistic as the material attributes (especially rigidity) incorporated into those simulations. Proven correlation between acoustic properties and material properties (especially stiffness/rigidity) is the basis for developing and implementing field-efficient, laterally continuous, non-invasive methods to accurately measure the seismic wave field.

Characterization of levees or dams in areas with liquefaction, core failure, or leakage potential would be enhanced if Poisson's ratio were calculated based on continuous, detailed, co-incident, two- and three-dimensional measurements of compressional and shear-wave velocities for cells uniformly distributed throughout the dam or levee volume. Routine non-invasive appraisal of dam/dike core integrity could prove quite valuable if lateral variability in shear-wave velocities could be accurately measured and correlated to localized anomalous material zones. This would be especially significant if these anomalous zones indicated dissolution activity, non-uniform compaction/settling or fracturing/cracking from dewatering of expansive clays prior to surface subsidence, the formation of vertically extensive chimney features or piping, or fracture permeability through the core. Seismic techniques hold vast potential for imaging and measuring materials in a fashion suitable for evaluating levee integrity.

This applied research project was designed to evaluate the potential of several seismic methods to characterize the condition of levees built in the 1930s and 1940s along the U.S./Mexico border in Texas and New Mexico as part of an International Boundary and Water Commission (IBWC) program. During this component of the project, preliminary studies along a stretch of the Rio Grande River levee west of Las Cruces uncovered evidence of slope deterioration along the levee's river side slope at a location where neither construction nor subsequent drill data identified or even suggested unusual core conditions. The core's ability to act as an impermeable barrier under flood conditions that reach design freeboard heights needs to be evaluated at such an apparently susceptible location, especially considering the materials that compose the shell as well as core were locally mined from the predominantly sand and silty-sand alluvial flood plain. Various non-invasive interrogation techniques sensitive to changes in moisture content within the core needed to be identified and studied for possible use as reconnaissance tools during flood events that could threaten levee stability.

Research on levees at the Las Cruces site incorporated interrogations along the crest using a range of geophysical tools as well as surface inspections along the crest and slopes with drilling along the crown road. As result of these various surveys three sites were selected with different characteristics and from these three emerged the best candidate for a percolation test performed by artificially ponding water against the levee slope simulating flood conditions. By repeating different geophysical surveys at a rate consistent with a 36-hour rise and then associated fall from designed, freeboard changes could be associated with increased saturation and empirical determination of the degree of change. As a result, sensitivity to the various measured properties to this simulated flood event could be evaluated. The site ultimately chosen for this experiment was inundated with rodent burrows that could have easily served as highly permeable zones through the shell and possibly into the core.

By isolating and measuring changes or the effects of changes to physical earth properties using seismic methods it should be possible to both reduce the inherent problem of non-uniqueness

and lower the threshold of physical property change currently necessary for seismic methods to uniquely and confidently detect a change. Correlating and quantifying known changes in physical properties with observed variations in seismic data attributes should provide the basis for accurate characterization of earth materials with no *a priori* information. For that reason, comparing two data sets acquired with identical techniques and geometries—one acquired when the levee was dry and a second when the levee was exposed to full board water levels—is the most effective approach for evaluating the various methods' ability to detect and quantify infiltration of ponded fluids into the levee with the potential for piping through the core. Contrasting seismic data before and after changes in shell saturation should allow differences in data characteristics related specifically to the presence of water with maximum head at the core boundary to be identified and quantified, with a template developed for use of seismic methods as a reconnaissance tool on levees.

Program Objectives

Geophysics used during site characterization routinely involves relatively noisy measurements of earth properties, qualitatively incorporated into working subsurface models with ground truth provided by observational data sets (e.g., drilling, outcrop studies, etc.). Near-surface seismic data are no exception to this generality. The primary objective or product of most surveys of this type is the qualitative assessment of subsurface layer topography (Clement et al., 1997; Pullan and Hunter, 1990; Lankston, 1990). Travel-time structure maps or two- or three-layer velocity maps are typical interpretation products of seismic surveys. These seismic interpretation maps are routinely merged into borehole-derived geologic and hydrologic models based for the most part on highly subjective and very sparse data sets. These simplistic models are then used for ground-water monitoring and remediation, geologic hazard detection, or engineering design purposes in an intuitive, experience-based manner (Steeples and Miller, 1990; Miller et al., 1999).

Considering the wealth of information contained in the seismic wave field, seismic measurement or imaging data are routinely underutilized for site characterization (Steeples et al., 1995). Surface seismic techniques are generally limited to routine mapping and delineation of subsurface structures, layer topography, anomalies, and stratigraphic changes (Jongerius and Helbig, 1988; Miller et al., 1989; Goforth and Hayward, 1992; Miller et al., 1995; Shtivelman et al., 1998; Guo and Liu, 1999; Stokoe et al., 1994; Michaels, 1999). In many instances, several earth properties (Vp, Vs, Qp, Qs, layer orientation, and thickness) can be estimated from the seismic wavefield for each subsurface cell. Velocity is probably the parameter most consistently measured or estimated by all seismic methods. Q, which stands for quality factor, is a measure of seismic attenuation and is generally very difficult to directly measure. A single seismic shot record has the potential to be divided into multiple modes or combinations of modes and processed uniquely for each mode and wave type. One data set could be uniquely processed focusing on at least four different energy types (body waves: refraction, reflection, and tomography; surface waves: shear velocity and Q).

This applied research project evaluated the applicability of several seismic techniques to identify, delineate, and estimate the physical characteristics or properties of materials within and beneath a representative expanse of IBWC levees south of Las Cruces, New Mexico (Figure 1). It was important that some measure be established (qualitative if necessary) of the correlation between seismic measurements, conductivity

Figure 1. Survey site near Las Cruces, New Mexico.

measurements, and the physical condition (increased permeability zones related to fractures, joints, dissolution, or erosion) of the levee core. Several surface seismic measurements were made and analyzed using state-of-the art methods and equipment. As part of the phase II component of this study, a repeat survey was conducted immediately before, during, and after ponding and levee saturation. Methods evaluated include: (P) refraction, (P) reflection, (P) tomography (2-D turning ray), surface-wave dwell, and surface-wave dispersion-curve analysis (MASW) for shear-wave velocity.

- The delayed-time method of first arrival/refraction analysis was used along the 2-D profiles at the crest of the levee to look for variations in layer velocities (Vp) at the core/pervious fill contact, core/native earth interface, and any discrete velocity contrast within the first 30 ft below the base of the core along both crest and toe profile lines (Scott, 1973).

- Turning-ray tomography was used to define Vp and Vs for subsurface cells filling the space between the levee/ground surface and 30 ft below the base of the levee along the crest and toe profile lines (Lanz et al., 1998). Conventional turning-ray tomography and joint analysis of refractions and surface waves (JARS) was done to appraise their relative accuracy when appropriate (Ivanov et al., 2006).

- Multichannel surface-wave inversion techniques (MASW) have proven capable of detecting anomalous shear-wave velocity zones within and below fill materials (Miller et al., 1999). Application of this technique to differential fill and core integrity problems at levee sites with expansive clays provided key insights into and an increased awareness of areas with leak or failure potential.

- Frequency dwell experiments provided the opportunity to compare frequency-dependent changes in surface waves with physical properties and/or changes in properties. Mono-frequency sweeps several seconds long were produced and recorded using the dependence of surface-wave spectra on depth of penetration and the shear-wave velocity (Xia et al., 1999).

- High-resolution seismic reflection data from the crest 2-D profiles was studied to determine the feasibility of coincidentally estimating Vp and Vs, sensitivity of reflection wavelet attributes returning from the base and/or beneath the levee to variations in core permeability (cracks, burrows), and travel time variations (static) associated with wavelet delays through cracked and/or burrowed sandy core within closely spaced subsurface cells for use in detailed mapping of levee core properties (Batzle et al., 1999; Berryman et al., 1999). Unfortunately, no usable reflection energy was recorded at any of the sites from within the levee.

Tests to determine field efficiency, resolution potential, cost effectiveness, interpretability (signal-to-noise), processing requirements, and measurement accuracy were integral to each of the individual seismic techniques studies. It was the intent of this study to acquire single-pass full-waveform compressional- and shear-wave data and to process the individual components of each mode using methodologies appropriate for the particular energy arrival. Therefore, minimal acquisition effort would yield several redundant measurements of seismic properties using different parts of the wavefield.

In summary, the primary objectives set out from the onset of this project were to determine compressional- and shear-velocity distribution within the body of the levee and any relationship to levee permeability. Measurements were made at several locations, each with unique physical and/or lithologic differences, while in their dry state to a depth approximately equal to the water table (geophysical tools used had at least a maximum depth of investigation extending 30 ft below the native ground surface or below the base of the levee). These measurements were followed some time later by an abbreviated comparison survey at a single site after water had been introduced to the levee core/body to provide a time-lapse seismic view of the levee, studying seismic response as a function of changes in saturation. As a result, the potential of reconnaissance and high-resolution imaging using non-invasive seismic methods could be appraised.

SITE DESCRIPTION

Levees along significant expanses of the Rio Grande River in south New Mexico are currently the responsibility of the International Boundary Water Commission (IBWC). Many of these levees were designed and constructed to minimize or eliminate the threat of the statistically determined 100-year flood event. Materials used to construct the levees were generally mined from barrow pits in proximity to the active construction area. Therefore, lateral variability in construction materials is common over distances of a mile or less. Average levee height in these areas is about 10 ft with slopes on the order of 1 to 3 (Figure 2).

With 11 years of prolonged drought conditions plaguing southern New Mexico, soil moisture conditions reached the point that concern arose about internal levee conditions and their impact on the levees' design characteristics. It was postulated that in some areas moisture levels within the levee could have dropped to the point cracks formed in the impervious core, weakening the core to the point failure was possible under 100-year flood conditions. A series of field tests were devised to first determine if a non-invasive method existed that could measure a levee's internal strength properties sufficiently to diagnose if this problem existed, and secondly to classify levees in terms of core characteristics. These investigations included seismic, ground-probing radar, resistivity, SP, drilling and sampling, and levee design-height (toe to within 3 ft of the levee crown) full-scale ponding tests. Data obtained prior to and after ponding tests were designed to assess differences at a single representative location that could be correlated to other sites with similar measured characteristics. This document is only intended to address seismic investigations undertaken by the Kansas Geological Survey (KGS).

Figure 2. Field site, crew working, and semi parked on levee.

Seismic investigations of this flood simulation were conducted at a levee site located in the La Mesa Quadrangle, New Mexico, USA (Figure 1). This site was selected after evaluating three different levee sites, all within a 1 km expanse along the southwestern levee structure. Seismic investigations were conducted at three levee sites located east of state Highway 28 (Figure 3).

In general, these sites are within the main floodplain of the Rio Grande River and situated on unconsolidated alluvial sediments (Figure 3). Gravels present within the alluvium at these sites included sedimentary rocks from the Cretaceous and Tertiary and a variety of igneous (including some agate) and sedimentary rocks from Trans-Pecos Texas, Mexico, and New Mexico. Surface materials at the sites are in an area classified predominantly as sand, fine, poorly graded. These distinctions could be important when considering the levees are generally constructed of locally farmed earth materials.

Surface investigations of the slopes and crests at all sites revealed more evidence of differences in material characteristics. Some of the levee segments had experienced invasion from small mammals leaving burrows 0.07-0.10 m in diameter.

A pond, approximately 30 m wide, was designed and built using earth material on the northeast side of a levee segment, which had burrows.

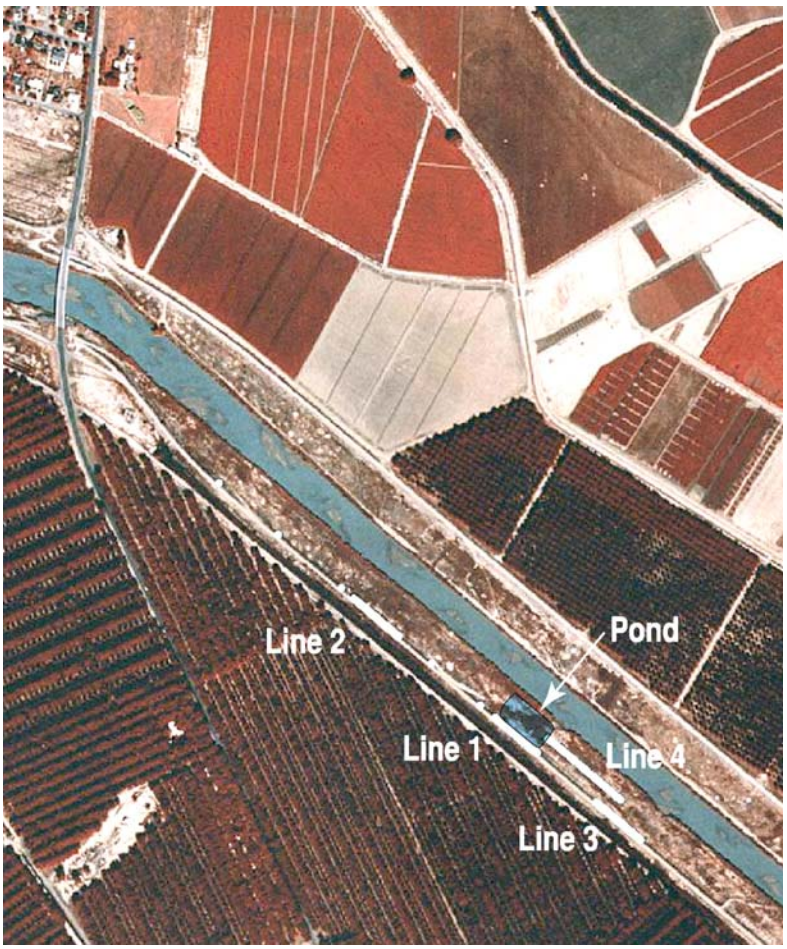

Figure 3. Aerial photo with GPS locations indicated for each line in the study area.

APPROACH

Refraction/Tomography

Direct and refracted P-wave and S-wave arrivals were analyzed using conventional methods (Palmer, 1981; Haeni, 1986; Lankston, 1990) and inversion techniques (Scott, 1977; Zhang and Toksoz, 1998; Ivanov et al., 2006). Use of direct and refracted arrivals for mapping distinct velocity contrasts between layers has been routine for everything from crustal seismic research (Steinhart and Meyer, 1961) to shallow ground-water studies (Haeni, 1978). It is an established, proven technique whose limitations are well documented (Soske, 1954; Sander, 1978). Methods to approximate solutions when physical conditions violate assumptions of the refraction method (Mooney, 1981; Redpath, 1973) are known. Recent research incorporating refraction inversion with shear-wave velocity calculations from surface-wave data has provided encouraging results that seem to be insensitive to the velocity reversal problem (Ivanov et al., 2006).

Tomography has a variety of applications in the subsurface, including: waste repository characterization (Peterson et al., 1985), engineering studies (Cottin et al., 1986), void detection

(Lytle and Dines, 1980), and mining (Kilty and Lange, 1990). The simplicity of acquisition and lack of computational intensity makes it especially applicable for velocity estimation using data acquired for surface-wave or refraction analysis. Using this approach in conjunction with multi-channel surface-wave inversion allows anomalous features within the levees to be examined all along the crest using shear and compressional waves. Processing data for tomographic analysis incorporated existing algorithms and standard curved-ray methodologies (Chiu et al., 1986).

Application of refraction (tomography) methods can be inaccurate due to the problem of nonuniqueness, meaning there are many possible solutions that can generate the same first-arrival values (Ivanov et al., 2005a). The Joint Analysis of Surface Wave and Refractions (JASR) method, developed at the KGS (Ivanov et al., 2006), offers an approach for minimizing one of the main problems in refraction tomography: nonuniqueness. A general way to overcome nonuniqueness is the use of *a priori* information. Such information generally comes from direct observations (borehole, outcrops, etc.). The JASR method obtains *a priori* information from Multichannel Analysis of Surface Waves (MASW) where a two-dimensional shear-wave velocity (Vs) section is used to construct a two-dimensional compressional-wave velocity (Vp) initial/reference model (*a priori* information for deterministic-type refraction tomography inversion). The validity of creating a Vp model from these Vs values is based on the common elastic and density parameters on which these two types of seismic velocities depend. Qualitatively this assumption is consistent with the frequently made observation that the general trend of Vs follows to the general trend of Vp. The JASR technique significantly improves the reliability of the final refraction-tomography inversion results (Miller et al., 2001; Ivanov et al., 2000; Ivanov et al., 2006).

Figure 4. Shear-wave source operated along the north line at site 2.

It was necessary to understand the arrival patterns of the various compressional- and shear-wave modes of levee refraction-tomography. Two-component data were recorded from a 2-D grid at the northeast side of the levee (Figure 4).

Surface-wave Inversion

Surface waves traditionally have been viewed as noise in multichannel seismic data collected to image targets for shallow engineering, environmental, and ground-water purposes (Steeples and Miller, 1990). Recent advances in the use of surface waves for near-surface imaging have combined spectral analysis techniques (SASW), developed for civil engineering applications (Nazarian et al., 1983), with multi-trace reflection technologies developed for near-surface (Schepers, 1975) and petroleum applications (Glover, 1959). The combination of these two uniquely different approaches to seismic imaging of the shallow subsurface permits non-invasive estimation of shear-wave velocities (within 10% of measured in many cases) (Xia et al., 2002) and delineation of horizontal and vertical variations in near-surface material properties based on changes in these velocities (MASW) (Park et al., 1996; Xia et al., 1999; Park et al., 1999).

Extending this imaging technology to include lateral variations in lithology as well as tunnel and fracture detection, bedrock mapping, and subsidence/karst delineation has required a unique

approach that incorporates SASW, MASW, and CDP methods. By integrating these techniques, 2-D continuous shear-wave velocity profiles of the subsurface can be generated. Estimating the dispersion curve from up to 60 receiving channels, spaced every 2 ft to 4 ft along the ground surface, enhances the signal and results in a unique, relatively continuous view of shallow subsurface shear-wave velocity properties. This highly redundant surface-wave method improves the accuracy of calculated shear-wave velocities and minimizes the likelihood that irregularities resulting from erratic dispersion curves will corrupt the analysis in comparison to the more traditional SASW approach.

Surface-wave analysis was performed on data acquired on the crest of the levee and on adjacent crest lines before and during the ponding experiment. Each of the three profiles located at different places along the levee and the profile used for the water flood experiment used the same spread geometry (120 stations with both compressional and shear receivers located every 2 ft) and permitted correlation between the various processed data sets for each line and between the three different lines. Even with the unique broadband requirements of surface-wave measurements it was not necessary to use an accelerated weight drop source, a hammer was sufficient (broad enough bandwidth, low enough frequency, and high enough energy), but low-frequency receivers and windowed processing was necessary to produce the highest quality results. Shear-wave velocity maps generated along each profile line were optimized for resolution and signal-to-noise. Several unique approaches were used to minimize smearing resulting from variable wavelength averaging.

Reflection

Seismic reflection is a powerful geophysical tool, in use since the 1920s that uses sound energy for underground exploration (Coffeen, 1978; Waters, 1987; Dobrin and Savit, 1988; Telford et al., 1990; Sheriff, 2002). For most of the first sixty years seismic reflection surveys targeted rock layers of petroleum interest at depth generally exceeding 1 km. Using seismic reflection techniques to image targets less than 100 m has only been attempted with published success since the 1980s. Key to using seismic reflection to image shallow targets is the production and recording of high frequency signal. Most recently the technique is finding new applications characterizing geologic and hydrologic settings at depths between 3 and 30 m below the ground surface.

High-resolution seismic reflections have been used to map shallow subsurface conditions for applications in geology, geotechnical, hydrogeology, environmental, mineral exploration), and petroleum exploration. Use of this tool to solve near-surface problems has escalated over the last 25 years, with exponential growth occurring over the last 15 years as the computer revolution has moved into full swing. Applications have predominantly focused on mapping, detecting, and/or delineating geologic conditions. Favorite targets of high-resolution seismic practitioners over the last couple of decades have been the bedrock surface, confining layers (aquitards), faults, lithologic stratigraphy, voids, water table, fracture systems, and layer geometry (folds). The petroleum industry has been the primary beneficiary of seismic reflection imaging and has poured millions of dollars into research and development and production application of the tool over the last 70 years in their search for rock layers that might contain petroleum reserves.

Analysis of data acquired at each of the levee sites will include processes specific to reflection as well as first arrival and surface waves. A separate reflection study was undertaken at the toe of the pond dam during the flood experiments in search of evidence the increased head from the pond would affect the water table elevation and seismic texture. It was our intent to concentrate

on: 1) generating high resolution (>250 Hz P-wave and >120 Hz S-wave) signals; 2) optimizing acquisition and processing for 2-D imaging along crest and toe without compromising first-arrival analysis, which was a higher priority operation; 3) establishing equipment configurations and parameter settings to maximize signal-to-noise and resolution potential considering the first-arrival acquisition deployment; 4) correlating P-wave reflections with S-wave reflections as well as with the other seismic, EM, and drill/excavation data; 5) performing attribute analysis of reflection waveforms passing through core, as well as careful study of velocity distribution calculated from NMO curves; 6) tailoring processing flows for non-optimized acquisition equipment and parameters due to full wavefield acquisition approach; 7) correlating compressional- and shear-wave NMO velocities for specific reflector(s); and 8) integrating reflection data with other seismic data. Source spacing, geophone spacing, line orientations, imaging, interpolation requirements, and fiscal constraints were to also be addressed, but due to limitations imposed as a result of coincident acquisition of first-arrival and surface-wave data, it was not possible to optimize both. Parameter and signal requirements are markedly different between the methods. Well-established shallow high-resolution data acquisition methodologies, emphasizing correlation of modal data and optimized velocity control, were adhered to as closely as possible without compromising other seismic methods (Hunter et al., 1984; Knapp and Steeples, 1986; Steeples and Miller, 1990).

DATA ACQUISITION

Phase I (data acquired during trip 1 from July 18-22, 2005)

Initial studies at the three sites were designed to identify any seismic characteristics unique to—or that could be correlated with—specific material characteristics interpreted to be indicative of structurally weak or more permeable zones. This research program was intended to evaluate as many seismic methods as possible and appropriate on the crest of these predominantly sand levees to determine the range and level of sensitivity the methods have identifying areas susceptible to core erosion and levee failure. Single data sets were acquired with the intention of separating and processing the individual components of the wavefield with appropriate methods and portion of the seismograms.

Consistency in recording equipment and parameters was critical for site-to-site comparison and especially for time-lapse studies of the kind planned here. A Geometrics 240-channel StrataView seismograph system was used to record all the seismic data for this project (Figure 5). The system is mounted in a 6-wheel John Deere Gator for added mobility and minimal environmental impact (Figure 6). This 24-bit A/D recording system used a Geometrics StrataVisor controller for basic QC and data storage. Throughout the project the same recording system was used, configured appropriately for each data set, and configured consistently for each data type. Consistency in acquisition from site to site and from survey time to survey time was a high priority that allowed broader assertions about the significance of the observed seismic differences and their relationship to the different physical characteristics and make-up of the levees at each site and with induced physical changes at an individual site. Since it was not clear from the onset which method or levee property would prove to be most sensitive to or indicative of levee degradation potential associated with the fine silty-sand material these levees were composed of or surface deterioration (such as the burrows observed at one site), all seismic methods and data modes had to be evaluated.

Initial testing at site 1 was completed first to measure some of the basic seismic characteristics and define the optimum equipment and configuration for data recorded on the crest of these levee structures in this area (Figure 3). Analysis of test data concluded 10-Hz single geophones, a

Figure 5. Geometrics 240-channel seismograph mounted in John Deere Gator.

Figure 6. Seismic data acquisition.

16-lb sledgehammer, three impacts per station, and planted geophones were optimum for both the surface-wave and compressional-wave tomography. Included in the testing regimen was evaluation of land-streamer data, 12-lb and 20-lb sledgehammers, 4.5-Hz geophones, and a mechanical weight drop.

At each site, one 2-D, 2-C profile was acquired along the crest of the levee (Figure 7). Receiver station spacing was 2 ft with two receivers at each location (10 Hz compressional-wave geophones and one 14 Hz shear-wave geophone) (Figure 8). Shear-wave receivers were oriented to be sensitive to motion perpendicular to the axis of the levee (transverse). A 16-lb sledgehammer impacting a striker plate of similar weight for compressional- and surface-wave data (Figure 9) and a 6" x 6" wood block outfitted with steel endplates and serrated earth-coupling teeth (Figures 10 and 11) were used for shear-wave data. The total spread length was 240 ft with 120 channels recording compressional and 120 channels recording shear signals. Source spacing through the spread varied, depending on data quality, from every 4 ft to every 24 ft. Each profile was acquired twice, once with the source in compressional-wave orientation and a second time with a shear-wave source orientation. Data were recorded from shear-wave phones when the shear-wave source was used and compressional-wave phones when the compressional-wave source was used. Stations (source and receiver) were located initially using analog measuring tapes/chain, followed by highly accurate (±1 inch) x, y, and z measurement using a Trimble DGPS surveying system (Figure 12).

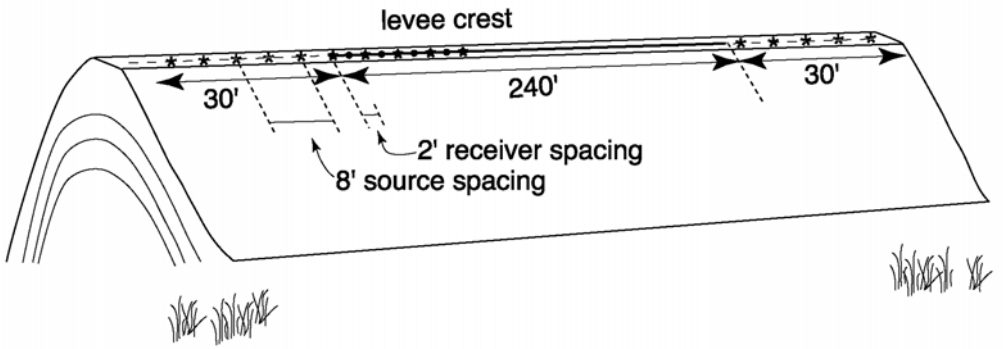

Figure 7. Crest seismic line deployment along river side of crown road.

Figure 8. Both compressional and shear geophones were used at each station.

Figure 9. Compressional-wave survey along levee crest road.

Figure 10. A 1-m-long wood block with steel end plates held down by standing on top of the block was used to generate shear energy.

Figure 11. Steel teeth were forced into the ground to minimize source decoupling and sliding along ground surface.

Figure 12. Differential Global Position System (DGPS) was used to accurately locate all sources and receiver stations.

Figure 13. IVI Minivib.

Vibrator dwell experiments were run at sites 2 and 3. These experiments were designed to measure any non-uniformity in the surface-wave propagation that might relate to variable mechanical or hydrologic properties of the subsurface unique to each site. An IVI minivib1 was used as the source for experiments both at the crest and toe (Figure 13). Receivers used for the compressional-wave 2-D full wavefield recording (single 10-Hz GeoSpace geophones) were the same as used for the vibrator dwell experiments. Shot stations for the vibrator experiments were located immediately off each end of the 120-station receiver spread.

Phase II (data acquired during trip 2 from September 14-15, 2005)

The second trip focused on the ponding experiment carried out at site 1 (Figures 14 and 15), based on the analysis of data acquired during the first visit. A water-retention structure was built at site 1 to allow the simulation of a flood event across a portion of the levee suspected to be

Figure 14. Pond constructed to test flood simulation interrogations.

Figure 15. Water pumped into pond at rate consistent with model flood.

susceptible to internal erosion and potential failure (Figure 16). This experiment was intended to determine if burrows in the fine-sand core, due to small-mammal activity, and lower shear wave velocities relative to the other sites tested support rapid piping and levee deterioration. Site 1 was selected based on burrow observations, drilling, conductivity measurements, and seismic properties. This phase of the project was designed as a time-lapse experiment where differencing could be used to investigate change in seismic properties that might occur as a result of increased saturation of the permeable shell and changes in the material property as a result of piping on the core.

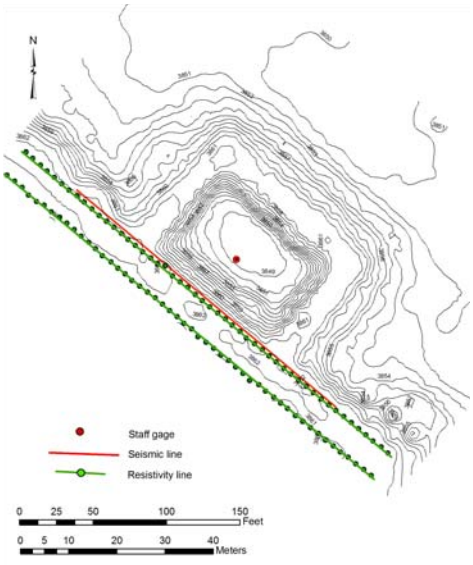

Figure 16. Sketch of test pond showing locations of seismic and resistivity lines along the levee crest.

The survey line was deployed along the northeast edges of the crest (Figure 17). Each receiver station had a 10-Hz compressional-wave geophone (Figure 18). Each

Figure 17. Seismic lines deployed along the northeast side of crest road at site 1.

Figure 18. Compressional and shear phones used for monitoring experiments.

Figure 19. Pond prior to the ponding experiment.

Figure 20. Pond was incrementally filled to simulate rising water from Rio Grande flood.

Figure 21. Pond nearly full.

Figure 22. Pool monitored with water added about once an hour.

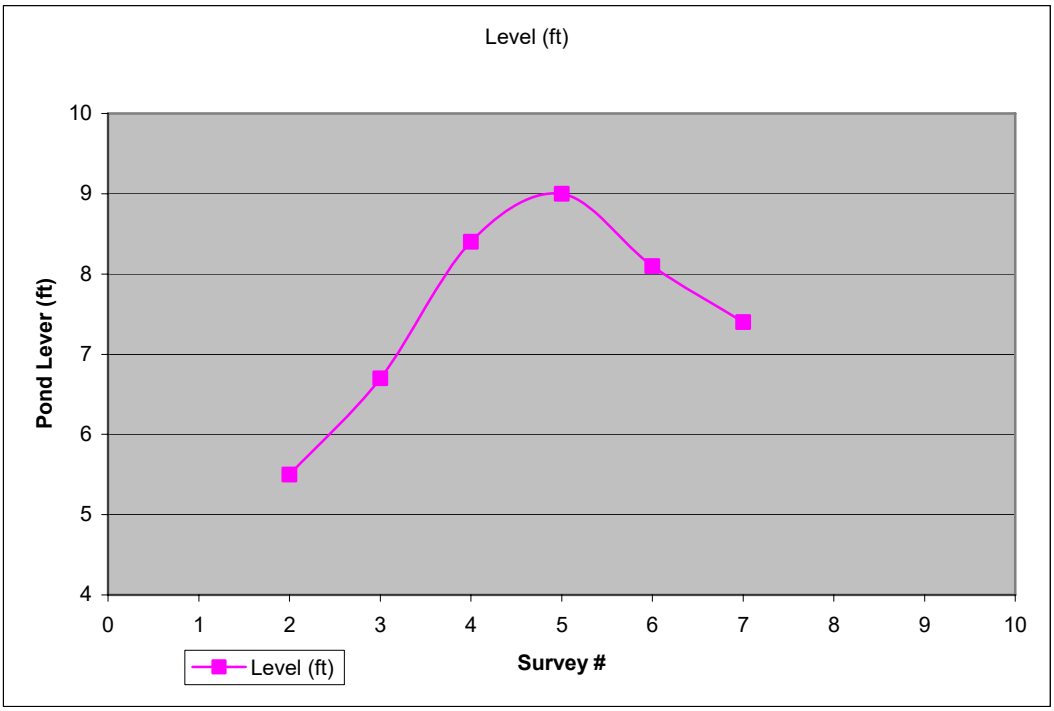

Figure 23. Water level for each of the surveys during the ponding experiment at line 1.

mode and profile was recorded for a given survey time. A baseline survey was acquired prior to water being in contact with the levee sides (Figure 19). Subsequent surveys were acquired while the pond was being filled (Figure 20) and retained at full board (Figures 21 and 22). Day 1 baseline data included hammer and compressional-wave vibrator. Three time-lapse data sets were acquired at about 4-hour intervals while the pond was filled from the river. The fifth survey was obtained 12 hours after the start of the experiment (Day 2) when water was at simulated full pool (9 ft). Pool level dropped to 8.1 and 7.4 during the next 8 hours (and was restored to full pool height) (Figure 23). Time-lapse seismic data were recorded four more times on 4-hour intervals.

For all data acquired with the sledge-hammer, each shot station and energy mode retained the field operator from beginning to completion. Three different hammer operators rotated off in a set order and at consistent shot stations. Comparison of recorded amplitudes was possible through time for a given configuration and energy mode because of this uniformity in energy and operational procedures. Maintaining a schedule with the designed uniform survey intervals required some night operations (Figure 24). Floodlights were used with associated generator noise during preparation, but the surveys were acquired noise free, with all pumps and generators turned off.

Figure 24. Night acquisition was necessary to capture water at key levels.

Changes in seismic velocities between the baseline survey at site 1 during the ponding experiment and reconnaissance surveys several months earlier is attributed to saturation differences due to higher than normal rainfall. The observed increase in seismic velocity was not site-specific variability or inconsistency of methodologies. Crest profile data for site 1 were acquired using as near-identical parameters and equipment as possible for both the reconnaissance and time-lapse surveys. Stations were located as closely as possible using landmarks and GPS locations established during reconnaissance survey.

QA/QC

The data acquired and processed on this survey were managed to ensure the highest quality and most accurate acoustic representation possible at this geologic setting. Current state-of-the-art techniques were used in a fashion that was appropriate and verified with step-by-step QA/QC. The most important (possibly even essential) QC information are samples of shot gathers. Raw and processed shot gathers allow geophysicists and geologists to determine the authenticity of processed seismic sections. Seismic processing software and techniques are very powerful tools that, if not used properly, can and most likely will result in unrealistic interpretations.

The equipment and recorded data were continuously monitored during acquisition to ensure the highest quality sections. Receiver response and sensitivity were monitored using a modified tap test performed after the planting of each geophone or group of geophones. The continuity and leakage of each active station was monitored prior to each shot. The system was subjected to a series of pre-acquisition tests designed to ensure consistency in system noise and precision in digitally stored data. Visual analysis of general signal-to-noise ratio, environmental noise, DC bias, and variations in the optimum recording window were performed on at least every fifth field plot. Preliminary in-field processing provided excellent insights into data quality and need for real-time parameter adjustments as well.

Data Storage

Data were recorded and stored initially on the seismograph controller hard drive in SEG2 format. At the conclusion of each day's work the data were downloaded via Ethernet to computer hard drives located in the Mobile Processing Center (MPC). Once on computers in the MPC at the field site, the data were converted and viewed to verify data were fully readable and error free, archived in SEG2 format on DVD media (media was read verified with two copies burned), and processed for preliminary infield analysis. These DVD media are now archived at the KGS in the seismic data library. Processing of the data required reformatting into a fixed modified SEGY format.

DATA PROCESSING

Overview and Processing Objectives

Trip 1 – July 18-22, 2005

Each data set was acquired with the intent of capturing a specific mode (compressional or shear) and positioned to target certain types of energy (Rayleigh wave, reflections, refraction, first arrivals, etc.) while focusing on a particular distribution of seismic characteristics (time-offset [t-x], frequency-wave number [f-k], frequency-phase velocity [f-v], frequency-amplitude [f-a], etc.). For each site there are two unique data sets for the crest; a compressional-wave survey and coincident shear-wave survey follows the same line. Several experiments were run using cross-modal data sets. These include acquisition using shear-wave receivers and a compressional-wave source and vice versa. Some of these more obscure data sets were not processed during this initial round of processing but were scheduled for later, more advanced processing runs.

Trip 2 – September 14-15, 2005

Design and construction of the water retention pond used for the flood simulation experiments was physically located as near site 1 from the reconnaissance trip as possible and in an area noted for excessive rodent burrows into the shell of the levee on the river side. If piping did occur, the experiments were set up to study the seismic changes and characteristics during fluid percolation into and through the core up to immediately prior to failure of the levee. Failure never occurred, so it is not clear how to relate and extrapolate the observed seismic changes with the point of failure and, therefore, it is still not known how good seismic monitoring might be as an indicator or early warning of failure.

Data acquired along the northeast side of the crown road were processed to enhance changes in seismic velocities potentially related to changes in saturation. If effective, this approach could provide a method for tracking zones of increased saturation and/or leakage through the levee as head pressures increase with increasing pool height. Processing flows for tomography and MASW were maintained as close to identical as possible from one time lapse to the next to ensure changes observed were from velocity and not processing parameter variations.

Processing Software

Several processing packages were used to analyze these data, each with an emphasis on a specific energy type or travel path. For surface-wave analysis a commercial program called SurfSeis developed at the KGS for Multichannel Analysis of Surface Wave (MASW) processing was used (Park et al., 1999). Turning-ray tomography data were analyzed and displayed using TomoSeis, a collection of algorithms under development at the KGS for Joint Analysis of Surface Waves and Refraction (JARS) processing (Ivanov et al., 2006). Seismic reflection data processing was accomplished with WinSeis, also a commercial processing package developed by the KGS. Both compressional- and shear-wave data for each method were processed following the same approach and using the same software.

Data Processing Methods

Surface Wave

The surface-wave component of the seismic data was processed to estimate shear-wave velocity using the MASW method. By analyzing the fundamental-mode Rayleigh waves, a shear-wave velocity profile (1-D and 2-D) is produced that can be used to evaluate material stiffness or anomaly detection of ground materials usually shallower than 30 m, both applicable for either engineering or geophysical projects.

The *SurfSeis* processing procedure consists of four steps:

1. Field setup—This encodes the surface location of seismic source and receivers into the field data.
2. Extraction of dispersion curves—Dispersion of the fundamental-mode Rayleigh wave is extracted from the seismic data.
3. Inversion for shear-wave velocity (Vs) profiles—Extracted dispersion curves are inverted for the Vs profiles, each of which depicts the Vs variation with depth at a particular surface location.
4. Calculation of a pseudo 2-D Vs profile using an interpolation algorithm.

Processing surface-wave data for this project involved extraction of the optimum 30 or fewer traces from each 120-channel shot record, transformation to phase velocity-frequency domain, and inversion of the fundamental-mode dispersion curve to produce an estimate of the shear-wave velocity function relative to depth (Figure 25). These 30-or-fewer-trace gathers were analyzed using *SurfSeis*. Each shot gather generates one dispersion curve that is assigned a surface location corresponding to the middle point of the analyzed spread. Care was taken to ensure that the spectral properties of the t-x data (shot gathers) were consistent with the maximum and minimum f-v_c values (v_c is the phase velocity of surface waves) contained in the dispersion curve. Shear-wave velocity maps generated along each profile line were optimized for resolution using several approaches, including unblurring and slope filtering. Wavefield maps have been generated based on optimized receiver-spread offset for depths of interest and data characteristics.

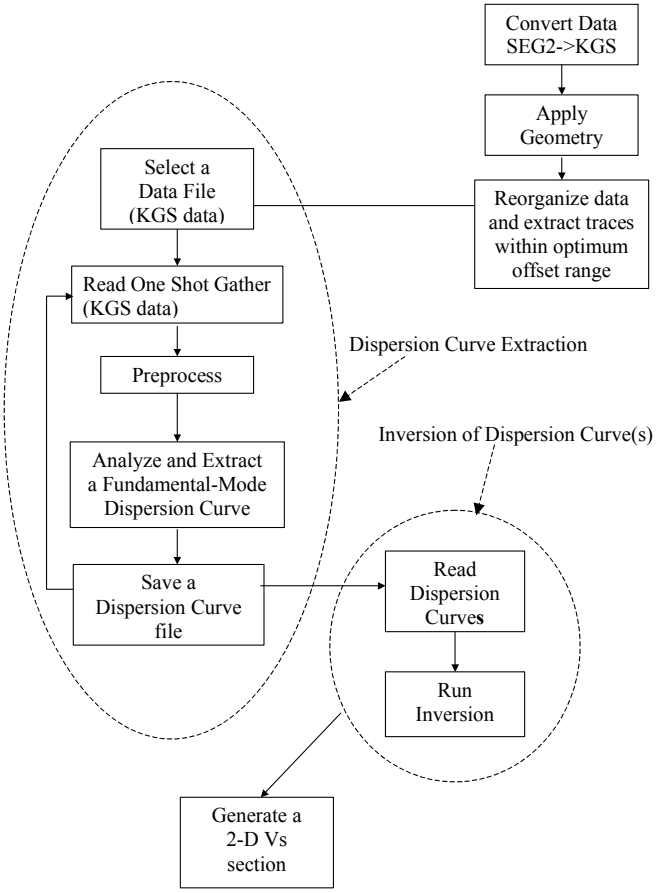

Figure 25. Processing flow for MASW data.

2-D First-arrival Analysis

First-arrivals were processed using the turning-ray tomography approach. This method uses continuous ray-path reconstruction and inversion to define the optimum velocity field beneath and between the source and receiver locations. Each subsurface cell has an optimum compressional-wave velocity assigned such that, when all the cells a ray penetrates between source and receiver are summed, the travel time is consistent with the time of the observed first arriving energy. For the work we present here a method called JARS was used to help eliminate problems of nonuniqueness inherent in most geophysical inversion problems. Incorporating the results of the surface-wave analysis permits *a priori* information to be included for construction of an initial reference model.

TomoSeis (under development at the KGS) analyzes first arrivals picked from seismic data that are collected along a single line and recorded by a single shot gather. First arrivals can be either direct or refracted seismic energy. Since propagation of seismic energy through the earth can be approximated by a ray traveling through multiple cells, each with unique velocity characteristics, each specific velocity set (all cells along a travel path) represent the geologic model consistent with the observed seismic shot gather. The inverse refraction traveltime problem can be solved by finding a velocity model with first arrivals that best match the observed first arrivals. However, the inverse refraction-tomography problem is nonunique and therefore many different velocity models can be valid solutions to the observed first-arrivals.

Two-dimensional Vs cross sections obtained from MASW analysis were used to generate an initial model for the tomographic inversion to Vp (Ivanov et al., 2006). Initial model optimization involves iterating an estimate of Poisson's ratio until model-predicted first arrivals correlate with those on actual shot records. Convergence of inversion runs required several iterations of the initial model, each time modifying conditioning parameters in a fashion appropriate for this data set (Figure 26). Optimization of the initial model was most efficient when best-fit conditioning parameters were used during preliminary analyses. Considering the resolution requirements and redundancy in rays penetrating each subsurface cell within the depth interval of interest, it was necessary for first arrivals to be picked for all traces on every shot gather.

By analyzing the correlation between model and observed data, it was possible to use final inversion results for quality control of the first-arrival picking routines. In some instances, secondary first-arrival analysis was necessary for convergence to a "good"

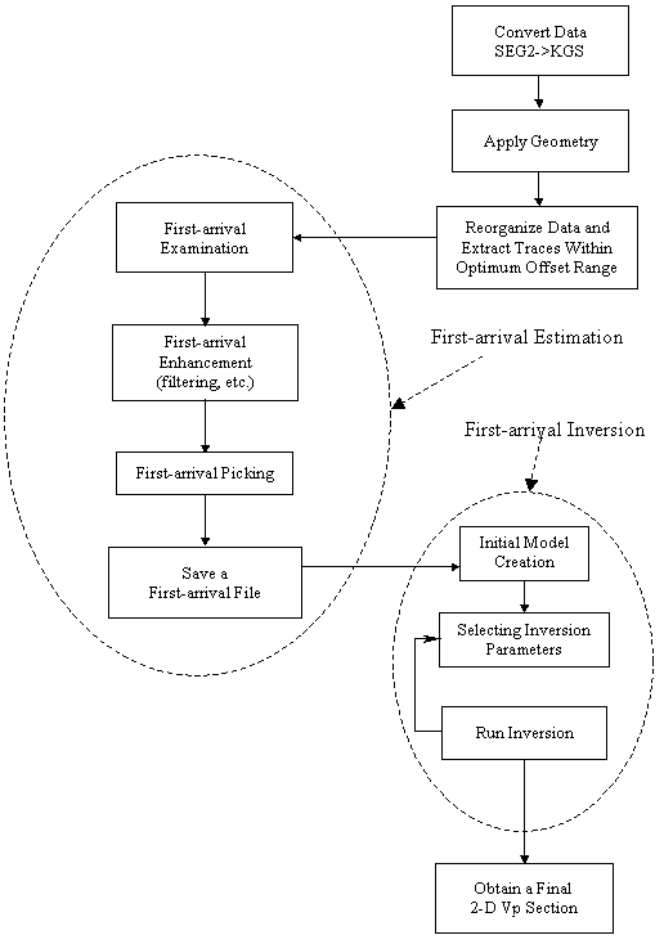

Figure 26. Processing flow for 2-D first-arrival analysis.

solution. Additional quality control was achieved by verifying that the 2-D Vp/Vs data were reasonable. *TomoSeis* was used to provide both traditional and JARS solutions to the 2-D refraction-tomography problem.

Reflection

Reflections from within and immediately below the basal levee contact were of interest and were the focus of reflection processing. High-resolution seismic reflection data, by its very nature, lends itself to over-processing, inappropriate processing, and minimal involvement processing. Interpretations of high-resolution shallow reflection data must consider not only the geologic information available, but also each step of the processing flow and the presence of reflection events on raw unprocessed data. Processing for the reflection portion of this study included only operations or processes that by their nature would enhance signal-to-noise-ratio and/or resolution as determined by evaluation of high confidence reflections interpreted directly on shot gathers.

Unfortunately, no primary reflection energy could be extracted from these data. With the focus of the acquisition more on first arrivals and surface waves, a very reflection-conducive setting would have been necessary for reflection returns from within the levee to be observed or enhanced through processing. For the most part, processing of high-resolution shallow reflection data is a matter of scaling down conventional processing techniques and methods; however, without extreme attention to details, conventional processing approaches will produce undesirable artifacts.

The basic architecture and sequence of processing steps followed during attempts to identify and enhance reflections was similar to conventional petroleum exploration flows (Yilmaz, 1987). The primary exceptions related to the step-by-step QC necessary for the highest confidence interpretations of shallow features and realization of full resolution potential (Miller et al., 1989; Miller et al., 1990; Miller and Steeples, 1991) (Figure 27). Specific distinctions related to the emphasis placed on avoiding processing techniques that through mixing, stacking, or filtering could either alias noise to appear as reflections or actually create artificial coherency. Data were processed using *WinSeis2* beta (next generation of *WinSeis*).

Figure 27. Processing flow for reflection data.

Display Formats and Presentation

Data are displayed in this report in a variety of formats, using several scales and color schemes. Each of the various seismic methods has a preferred or "normal" display format. The use of color and scales is generally a data-specific designation. Color is used throughout this report to enhance the dimensionality of the numerical data sets and to improve the apparent resolution of the data by focusing on the signal portion of the data.

Seismic data are recorded as digital words (representing amplitude of deflection or velocity) stored in a time-sequential order with uniform sampling rates. Sound waves are only useful for imaging if they are recorded over a finite time duration (also know as record length or recoding time). Considering that the velocity of sound in rock is generally several times to an order of magnitude or more greater than the velocity of sound in air, recording or listening times of fractions of a second are all that are necessary to fully capture the seismic wavefield from start (source impact/energy release) to finish (wavefield past the listening array). Analog display of seismic data is most commonly seen in what is referred to as wiggle-trace. In wiggle-trace format each sample is plotted as a function of time with a curve drawn through each sample forming a wiggle with the amount of deflection from the zero line equal to the amplitude of recorded signal.

Different components of the seismic wavefield are processed using very specific methods focusing on the particular characteristics of each different component. Initial surface-wave processing produces what is referred to as a dispersion curve. This curve is actually a trend in the data when displayed in frequency-phase-velocity space. A color scale indicative of degree of intensity or highest sample density is generally used to represent this pre-inversion data. Color contouring is a common display format for data that have gone through inversion. In this type of display, different colors represent different ranges of values; therefore, all areas with the same value will also have the same color. Velocity, as well, is generally represented using different colors for different ranges of values.

For most geologic applications, earth materials are generally considered to continuously change from one location to the next in a uniform and/or predictable manner. Since most seismic data are processed in a cell-by-cell or discrete fashion, to represent earth materials as realistically as possible it is necessary to interpolate between discrete sample points or cells. This process basically makes the assumption that the values between sample points transition between those points in a predictable fashion. This process of interpolation results in a smooth curve or transition across a digital data set. In its most basic form, a digital data field or plot can be contoured such that all points of equal value are connected with curves. This process allows areas with a collection of highs or lows to be easily identified and some degree of continuity in data trends established.

Merging of colors through the spectrum is a way of indicating gradational changes or transitioning of certain earth properties across a survey area. Trends associated with inferred material properties can be established and equated to known values or ground truth. Color contoured (each color representing the same value or level for the mapped property) data provide an image sensitive to changes in the displayed property and therefore allow a greater awareness of difference across a site and from survey to survey (assuming each color is assigned a fixed value that is consistent for all data sets displaying a particular property).

Discussion of Data and Processing at Each Site: Trip 1

A generally consistent set of data was recorded for each site with data processing also following a previously described relatively consistent flow with only minor tailoring for each site. Most of the site specific processing was necessary due to slight differences in acquisition parameters and/or methods that were used and/or evaluated for each site.

Seismic-data processing was designed to provide accurate and precise Vp and Vs earth models from the crest to depths significantly below the levee foundation. Comparison of key seismic properties were used as the basis to search for anomalous zones within the levee core that might be indicative of weakening beyond the level of performance as necessitated by construction specifications under the designed water load. As well, a Vp/Vs ratio map (reasonably consistent with Poisson's ratio) could be derived and used as an additional tool to search for areas of reduced strength within the levees. Larger Vp/Vs generally equates to weaker material from a ripability or shear strength perspective. With the levees constructed without a distinguishable core and with all native materials, little difference in measured seismic properties would be expected between the foundation and levee proper.

Line 1 Analysis

Estimates of cross-sectional Vs were obtained from the levee crest using tomography and surface-wave inversion techniques. Vp information was extracted from P-wave data using first-arrival analysis (tomography). Frequency dwell data were analyzed for amplitude variations as a function of frequency, specifically looking for changes in phase that could be related to changes in material seismic velocity.

MASW

Optimizing Surface-wave Analysis Trace-offsets Selection

To establish a general understanding of energy partitioning and model distribution we analyzed several representative shot records retaining all recorded traces. At this stage most of the processing effort was focused on distinguishing and classifying native dispersion-curve trends (Figure 28a).

The quality of fundamental-mode energy was appraised for six spread-offset ranges starting with the closest (6-60 ft), in which the fundamental mode and higher modes were blurred together (Figure 28b), and concluding with the long offset range 6-110 ft (Figure 28g). The 6-100 ft offset range (Figure 28f) was selected to be optimal for picking the fundamental mode of the surface wave. Greater offsets (Figure 28g) were not used to avoid degradation in the resolution potential thereby improving the lateral resolution of the survey.

Based on dispersion curve analysis the levee was principally interrogated by frequencies above 25 Hz. The wavelength for 25 Hz Rayleigh Wave energy was roughly estimated to be 450(ft/s)/25(Hz) = 18 ft, a wavelength theorized to mainly represent materials in the upper 9ft (using half-wavelength assumption). Furthermore, at 60 Hz the fundamental mode is at 350(ft/s)/60(Hz) = 6 ft wavelength = 3ft depth. Therefore, frequencies above 60 Hz would primarily provide information for the upper 3 ft of the levee crest. Guided by the previous observations the optimum spread selected for analysis was focused on fundamental-mode energy around and above 25 Hz.

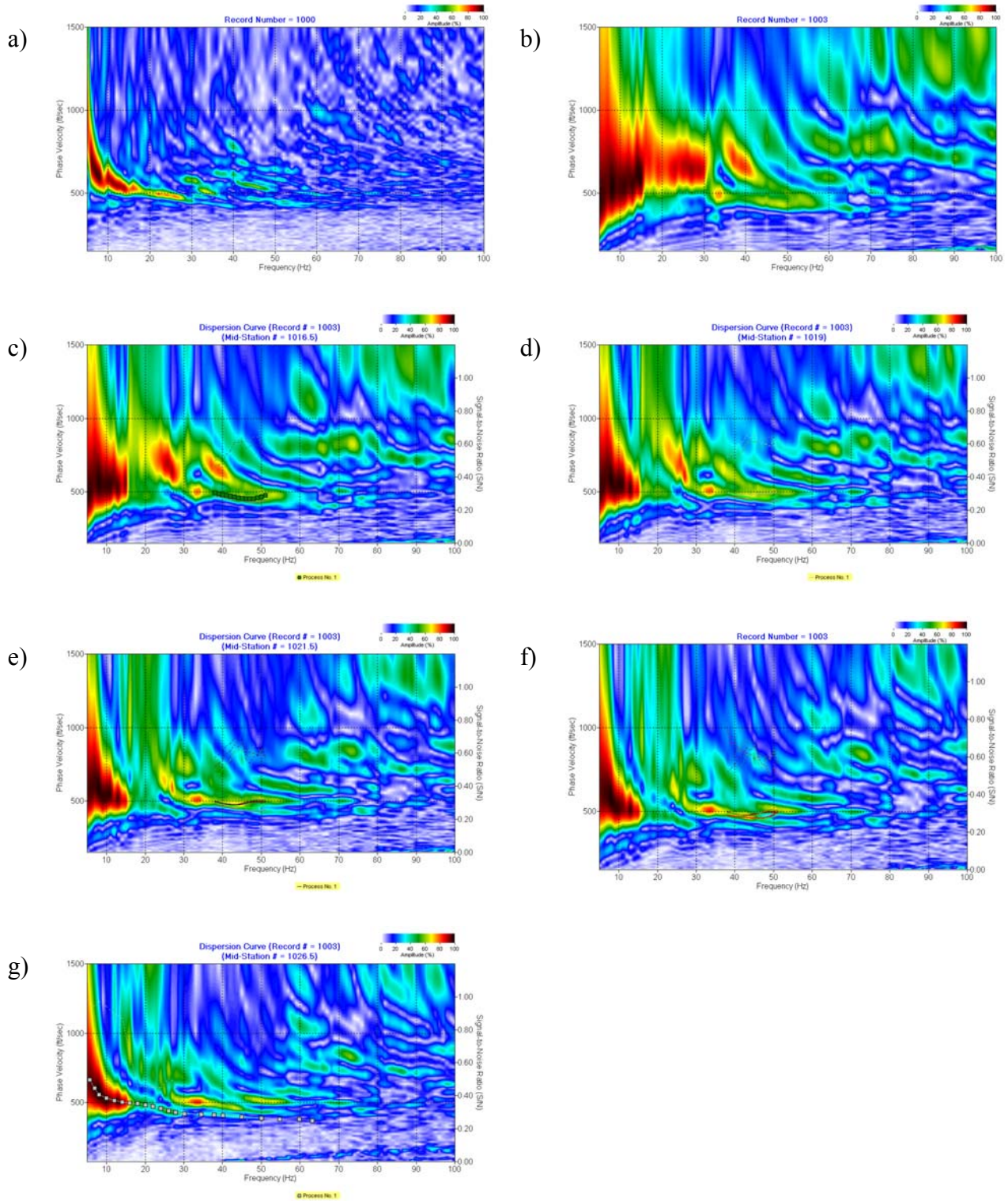

Figure 28. Phase-velocity – frequency transform of selected trace-offset ranges, a) all traces, b) 6 to 60 ft, c) 6 to 70 ft, d) 6 to 80 ft, e) 6 to 90 ft, f) 6 to 100 ft, g) 6 to 110 ft.

Traditional MASW Processing

Initially the dispersion curves were interpreted for all observed frequencies (6 to 80 Hz; Figure 29). The inversion results provided a 2-D Vs image for depths down to 60 ft (Figure 30). These results provided important guidance and information about the overall structure and characteristics of the sediments within the levee, foundation, and the majority of the unconsolidated sediments above bedrock, but provided little detail about the upper 10 ft that represented the levees themselves.

Levee-focused MASW Processing

To better focus and control the MASW method on the levees themselves we edited the dispersion curves, removing frequency components estimates to be less than 10 Hz. The lack of very low frequencies forced the software to use a shallow inversion model (max 26 ft deep). With this more depth-constrained approach the inversion model focused on the shallower portion of the line (Figure 31) providing a much better image of the internal characteristics of the levee.

Efforts to Improve the Levee Imaging

FDSE. The FDSE filtering method (Park et al., 2002) was tested to evaluate its effectiveness in removing the higher-mode energy that was interfering with the fundamental mode. The minimal separation in the velocity characteristics for the different surface-wave modes within the targeted frequency range (above 25 Hz to at lest 50 Hz) made it was especially difficult to apply FDSE to these data.

Muting Tests. Muting selective energy (Ivanov et al., 2005b) on representative records from Line 1 data showed great promise for improving the dispersion-curve picking confidence in the 25-90 Hz range, thereby imaging the confidence in the levee velocity structure (Figure 32). Conservative muting enhanced both fundamental and higher mode energy in the targeted frequency range of 25-50 Hz (Figures 32b and 32e). Thus, muting did not serve its primary purpose, namely the reduction and ideally the elimination of higher-mode energy. Furthermore, more aggressive muting preserved higher mode while the fundamental-mode energy suffered to the point of being barely traceable (Figures 32c and 32f). Three mute patterns were applied to all shot gathers from line 1 to provide dispersion curves that better estimated the fundamental mode.

We applied aggressive muting to all the shot records, specifically the dominant surface-wave energy. Seismic energy remaining after this liberal muting was analyzed in search of fundamental-mode energy. Dispersion curves were picked (Figure 32b) in the frequency-phase velocity domain after editing was completed in the t-x domain. Dispersion curves from the muted data set were then combined with the unedited, full frequency range dispersion curves. These combined dispersion curves were inverted using a maximum depth model (Figure 33). The obtained Vs results are nearly identical to those from the inversion using only the initially dispersion curve picks (Figure 30). To better focus on the levee itself a shallower model (max 26 ft deep) was used to invert the combined dispersion curves (Figure 34). The Vs results from this later approach provided no improvement to the levee image in comparison to the Vs from unmuted dispersion curves using the shallow model (Figure 31). More subtle muting provided little improvement to the inversion model and are therefore not displayed.

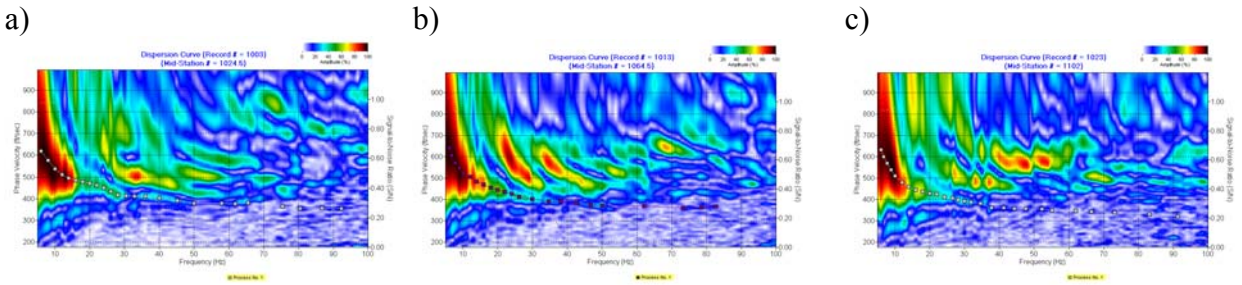

Figure 29. Line 1. Dispersion curve images extracted from the shot gathers located at the a) west end, b) middle, and c) east end of the line.

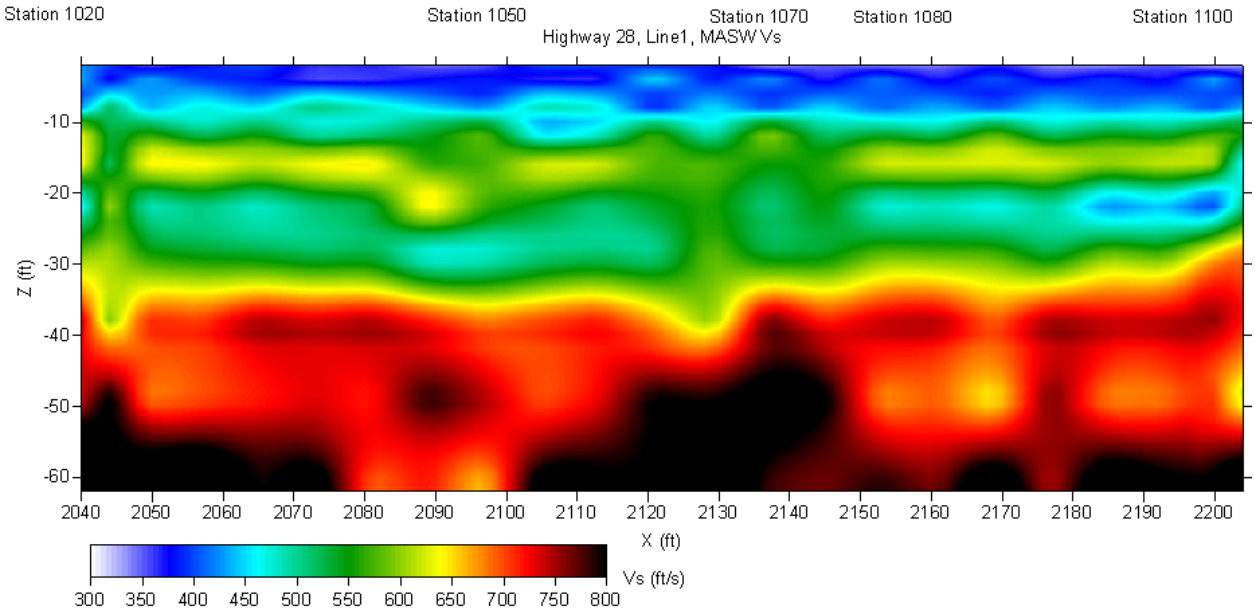

Figure 30. MASW Vs results for Line 1.

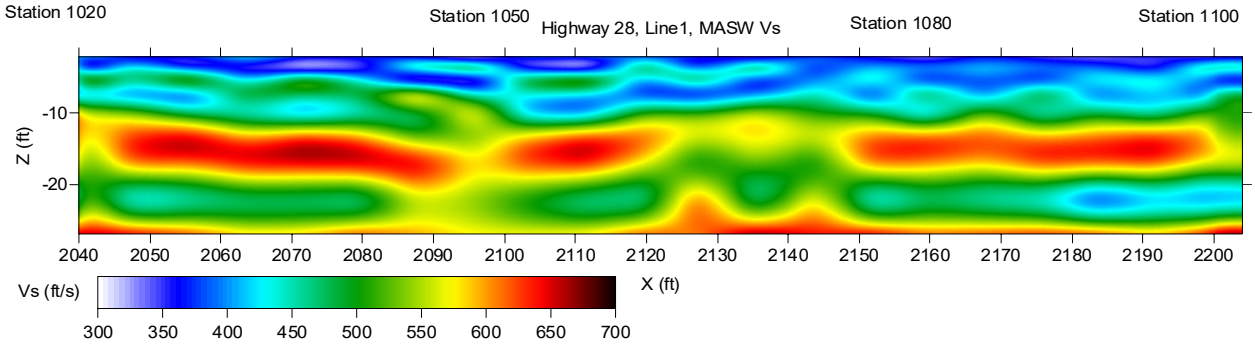

Figure 31. Shallow-focused MASW Vs results for Line 1.

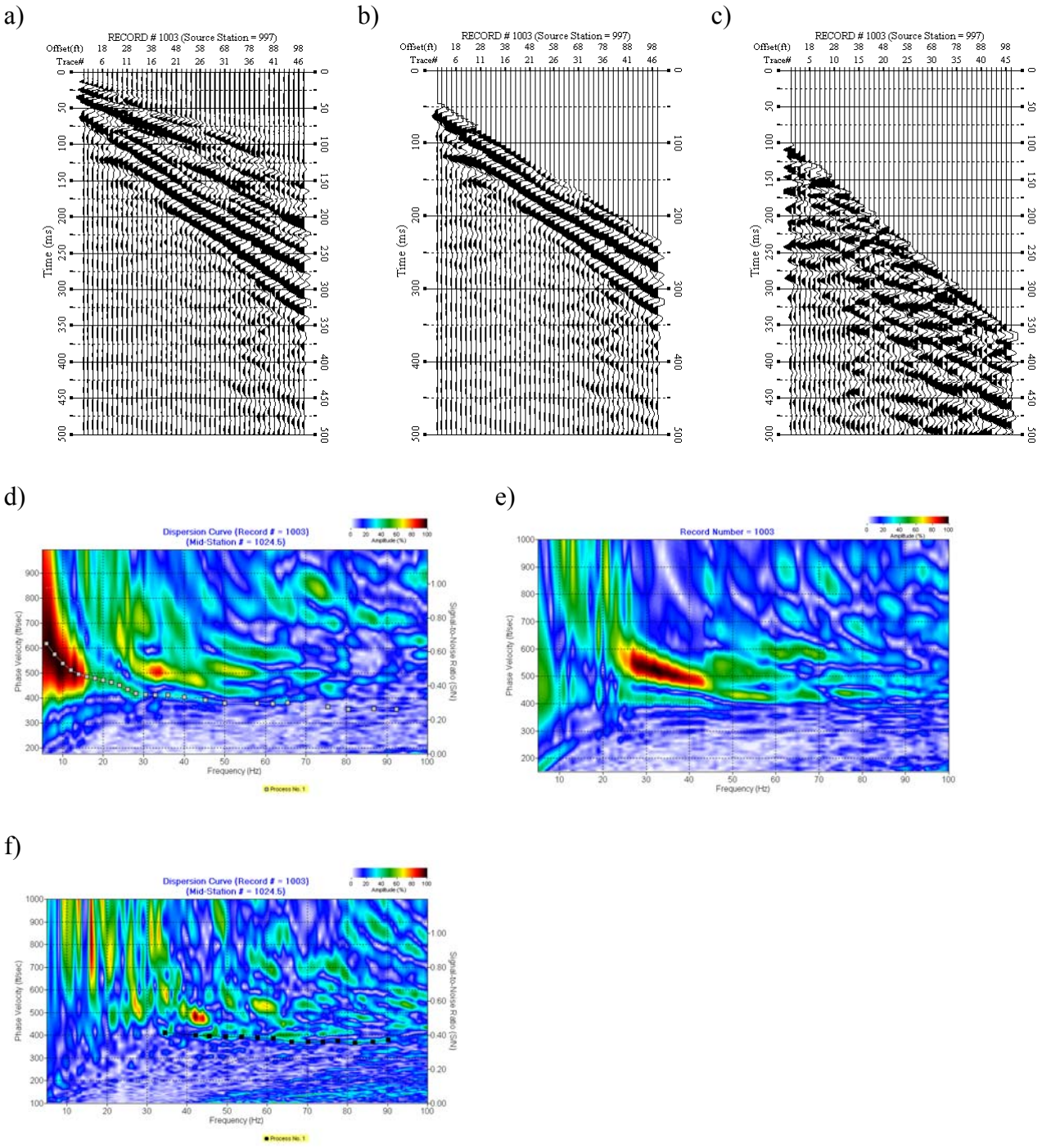

Figure 32. Testing muting on raw shot gathers of Line 1 to improve the dispersion curve imaging of the fundamental mode of the Rayleigh wave, a) raw shot gather, b) moderately muted higher mode, c) strongly muted higher mode, and their corresponding phase-velocity – frequency images d), e), and f).

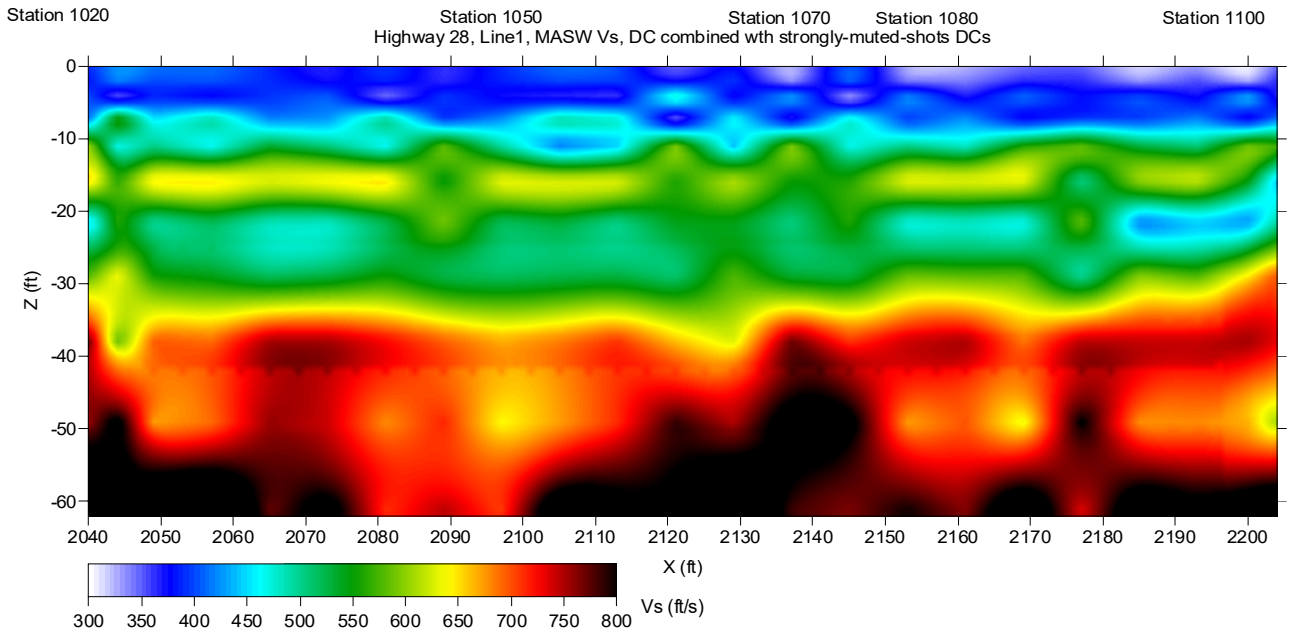

Figure 33. Line 1 MASW Vs results from combined dispersion curves, the higher frequency portions of which were estimated from the strongly muted data.

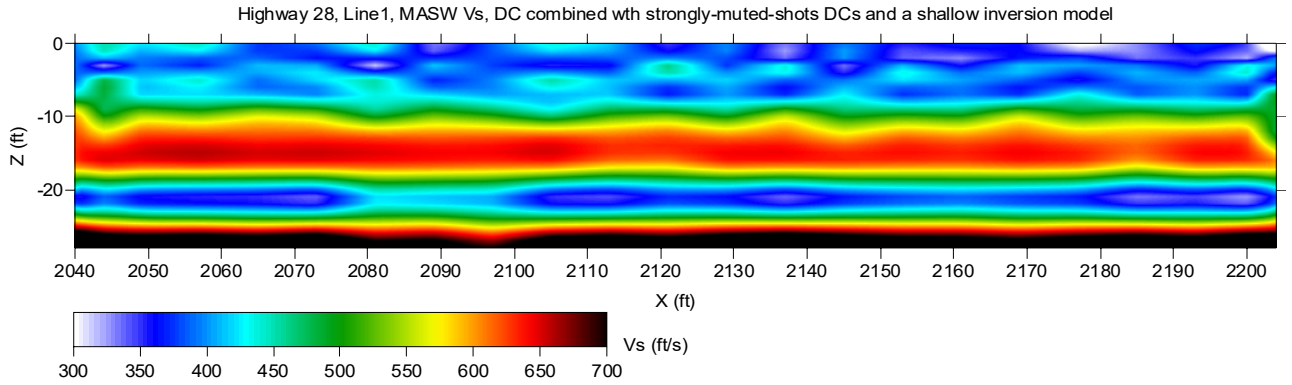

Figure 34. Line 1 shallow-focused MASW Vs results from combined dispersion curves, the higher frequency portions of which were estimated from the strongly muted data.

Reverse Line Processing

The MASW analysis on data with reverse shot-receiver orientation had weaker higher modes. Such a relative decrease of higher-mode energy allowed better fundamental- and higher-mode separation (especially between the targeted frequency range 25-50 Hz). This was accomplished by using a slightly longer spread length (110 ft [Figure 35] instead of the 100 ft used for the forward analysis). This benefit in mode separation observed after using a longer spread was not evident on the forward data (Figures 28f and 28g). Furthermore, subtle muting (Figure 36b) enhanced the targeted 25-55 Hz range of the fundamental-mode dispersion curve (Figure 36d). For comparison, subtle muting was ineffective in enhancing the fundamental mode image on forward data from the same location (Figure 37).

At present, it is unclear why it was easier to observe and separate fundamental-mode energy from higher modes on reverse line data compared to the forward line. In general, data acquired at sites such as this and in the fashion described here show some level of reciprocity.

Muting Processing of Reversed Line

Non-aggressive muting applied to all the shot gathers from the reversed data set made the fundamental mode easier to pick within and below the desired frequency range of 25-50 Hz (12-14 Hz) (Figure 38). This allowed dispersion-curve combinations and running a shallower model (half space at 25 ft) inversion to be avoided. The image resulting from this approach allows a significantly better interpretation of the top part of the levee (Figure 39).

P-WAVE FIRST ARRIVALS

First-arrival P-wave energy at each trace was picked automatically on shot gathers with minimal manual adjustments. These manual adjustments were necessary to compensate for slight variation in waveform and random noise (Figures 40 and 41). There are two distinctively different apparent first-arrival velocity trends based on trace-to-trace analysis of the P-wave data (Figures 40 and 41). From a basic refraction analysis perspective, the two distinctly different phase velocities (approximately 950 ft/s and 5500 ft/s) interpreted from these data are likely related material within the levee and the shallowest portion of native foundation (possibly the near-surface material [upper few feet of native sediments]). A 2-layer model solution (consistent with the two observed apparent slopes) places the depth of the high-velocity (5500 ft/s) refractor at about 18 ft. Refraction-tomography analysis provided a detailed 2-D Vp solution for line 1 (Figure 42). The 2-D solution represents a cross sectional slice of the levee, physically equivalent to cutting a slice parallel to the centerline (axis) of the levee, remaining one side, and observing the material cross-section from some distance away either north or south. This solution was obtained after minimal model iterations and provides an excellent match between the modeled and observed first arrivals. The 2-D Vp solution for line 1 was rescaled in both dimensions (x and z) to better focus on the levee and for ease of comparison with the rest of the results (Figure 43).

a) b)

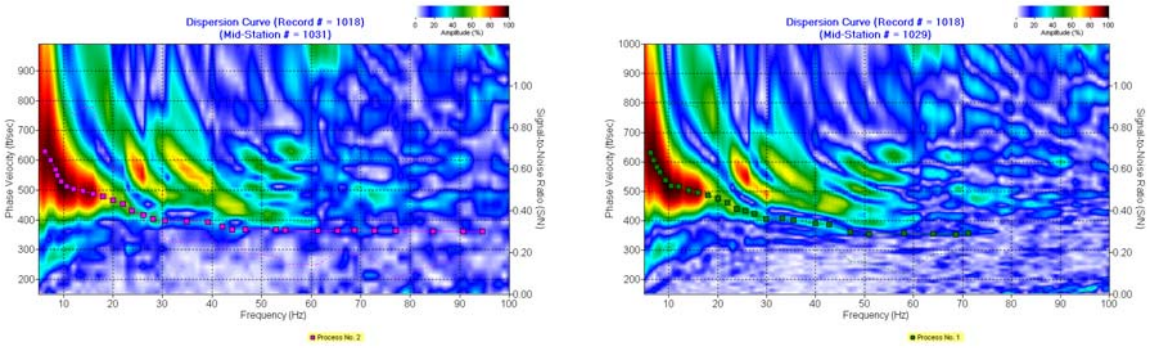

Figure 35. Line 1 reverse data. Phase-velocity – frequency transform of selected trace-offset ranges, a) 6 to 100 ft, b) 6 to 110 ft.

a) b)

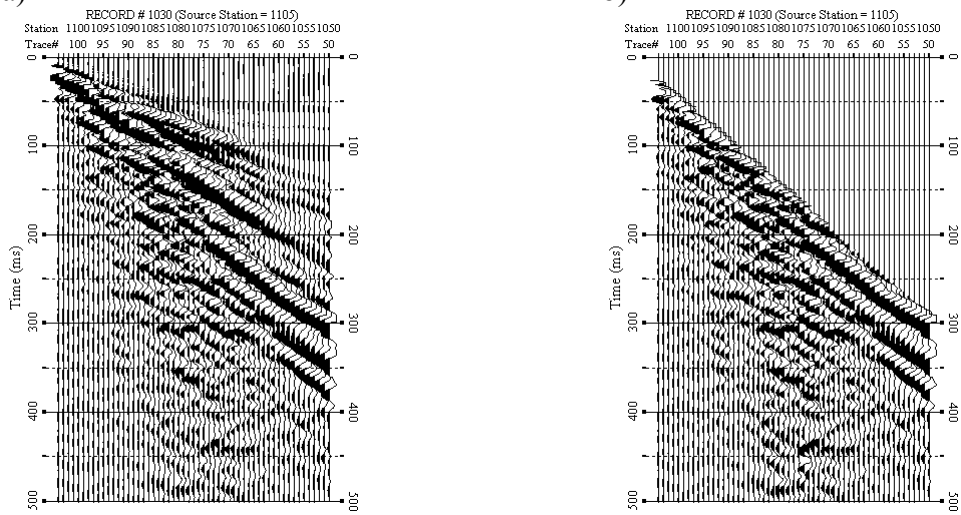

c) d)

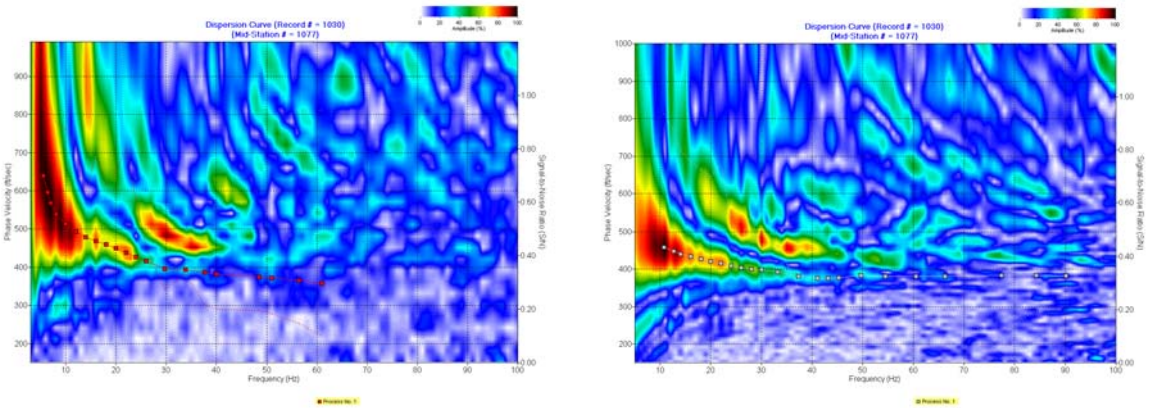

Figure 36. Line 1 reverse data. Mild muting b) on raw data a) improved the fundamental-mode energy between 25-55 Hz d) compared to the image of unmuted data c).

a) b)

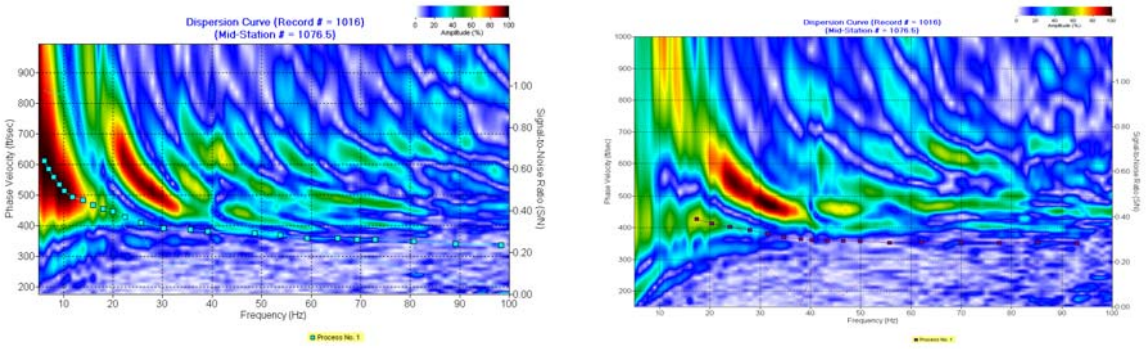

Figure 37. Line 1 forward data. Mild muting b) on raw data a) did not improve the fundamental-mode energy between 25-55 Hz d) compared to the image of unmuted data c).

a) b)

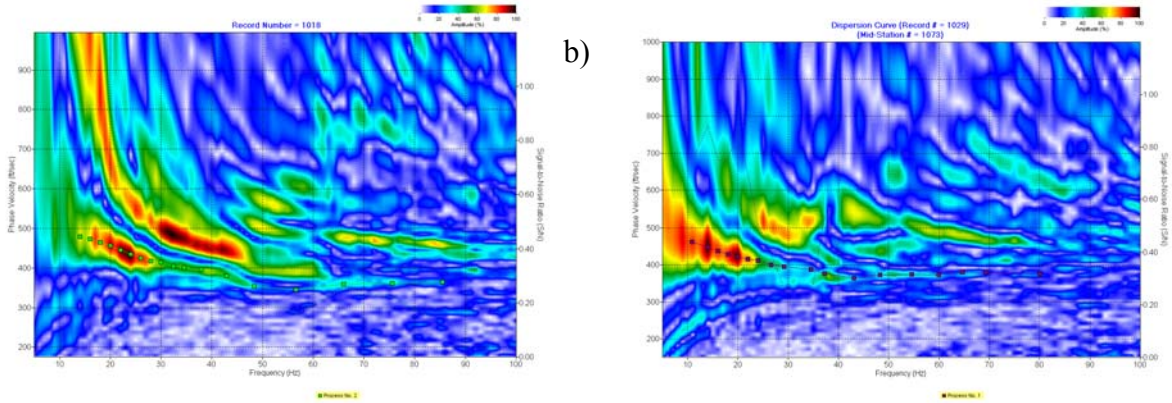

c)

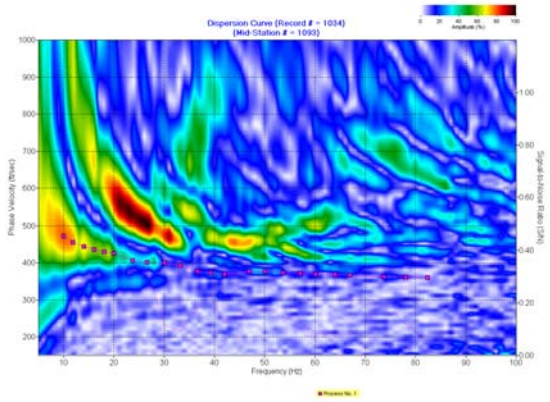

Figure 38. Line 1 reverse data. Dispersion curve images extracted from the mildly muted shot gathers located at the a) west end, b) middle, and c) east end of the line.

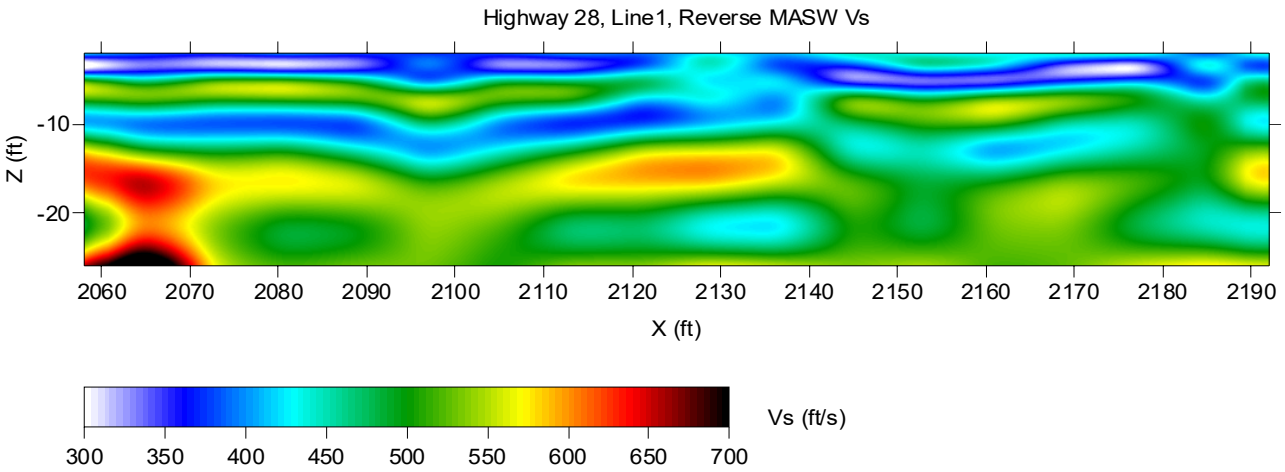

Figure 39. Line 1 reverse data MASW Vs results.

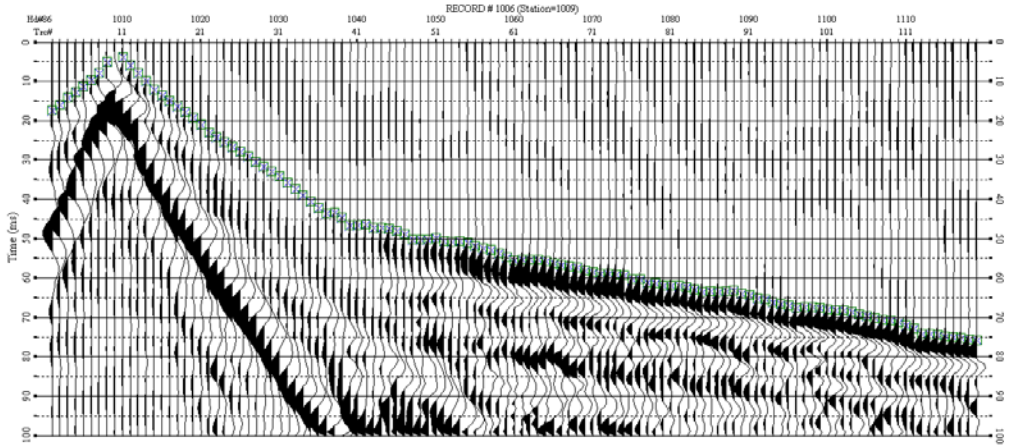

Figure 40. Estimation of first-arrival times on a P-wave seismic data with source located at station 1009 (horizontal location 2018 ft).

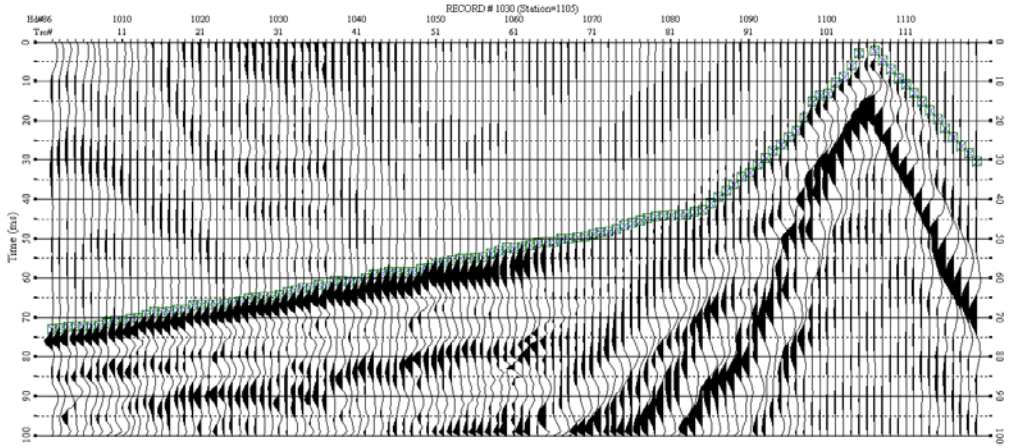

Figure 41. Estimation of first-arrival times on a P-wave seismic data with source located at station 1105 (horizontal location 2210 ft).

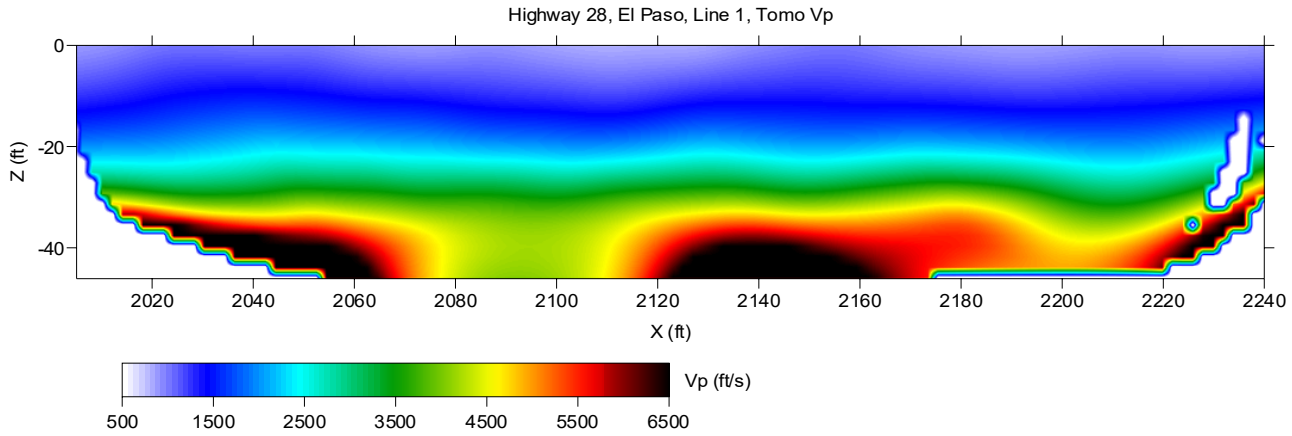

Figure 42. P-wave velocity model estimated for line 1 by analyzing P-wave data first-arrival times using refraction-tomography software.

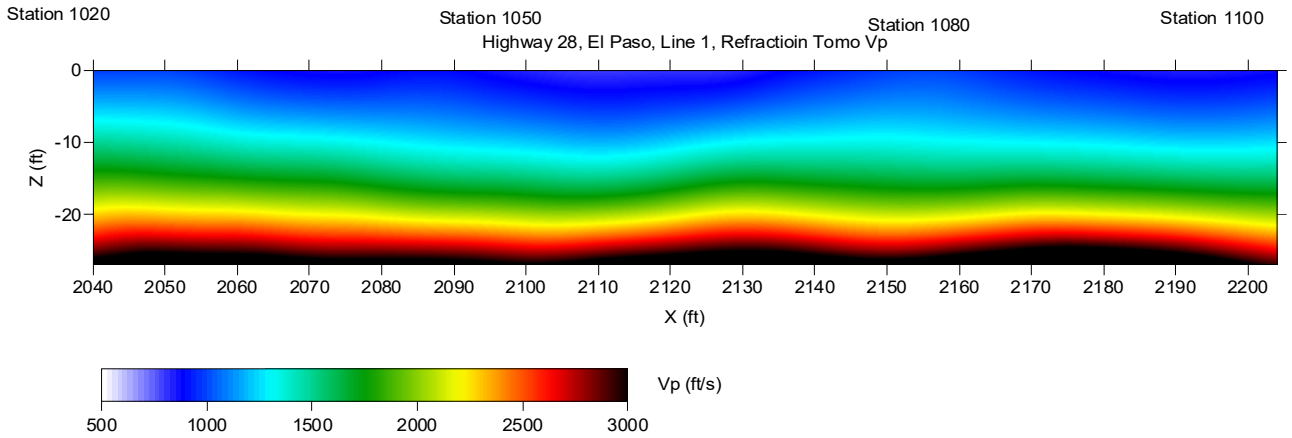

Figure 43. P-wave velocity model estimated for line 1 by analyzing P-wave data first-arrival times using refraction-tomography software rescaled for comparison with the rest of the Vp and Vs results focusing on the levee.

Line 2 Analysis

MASW

In contrast with the seismic data from line1 the fundamental-mode component of the surface-wave estimated on line 2 was strong enough that no additional filtering was required to estimate the dispersion curves within the targeted frequency range of 25-50 Hz (modeled to primarily sample levee material) (Figure 44).

Traditional MASW Processing

Following line 1 processing, dispersion curves were initially picked for all observed frequencies (6 to 80 Hz). The inversion results provided a 2-D Vs image as deep as 60 ft (Figure 45). These results provided important information on the overall structure and lithology of the sediments within that depth range but possessed little detail from within the levees, represented by the top 10 ft of the section.

Levee-focused MASW processing

Consistent with the inversion analysis and methodologies used on line 1, dispersion curves were edited to remove frequencies below 14 Hz to better focus the MASW method into the levees themselves. An improved levee image was obtained by using the same shallow inversion model (max 26 ft deep) to obtain a 2-D Vs section (Figure 46).

P-WAVE FIRST ARRIVALS

First-arrivals on shot gathers on line 2 had the same characteristics as on line 1 and were picked automatically with only a very few picks needing manual adjustments. Refraction-tomography processed sections provided a detailed 2-D Vp solution for line 2 (Figure 47). For these data the 2-D solution represents a cross sectional slice of the levee, physically equivalent to splitting open the levee parallel to the levee's centerline (axis). A solution was obtained with minimal model iterations that appeared to provide an excellent match between the modeled and observed first arrivals. The 2-D Vp solution for line 2 was rescaled to focus on levee material and for ease of comparison with the rest of the results (Figure 48).

Line 3 Analysis

MASW

Similar to the seismic data from line 2, the fundamental-mode components of the surface-wave were strong enough to permit estimation of dispersion curves within the levee within a frequency range from 25-50 Hz without additional filtering consistent with the pattern on Figure 44.

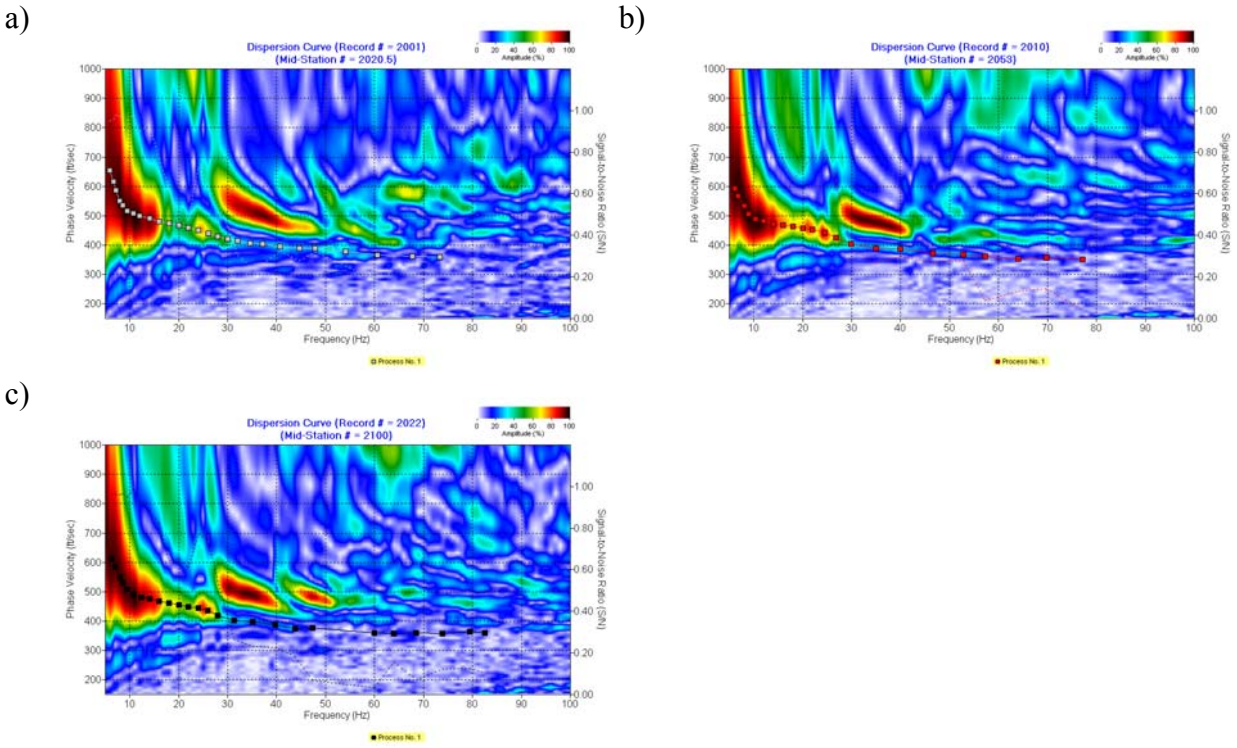

Figure 44. Line 2. Dispersion curve images extracted from the shot gathers located at the a) west end, b) middle, and c) east end of the line.

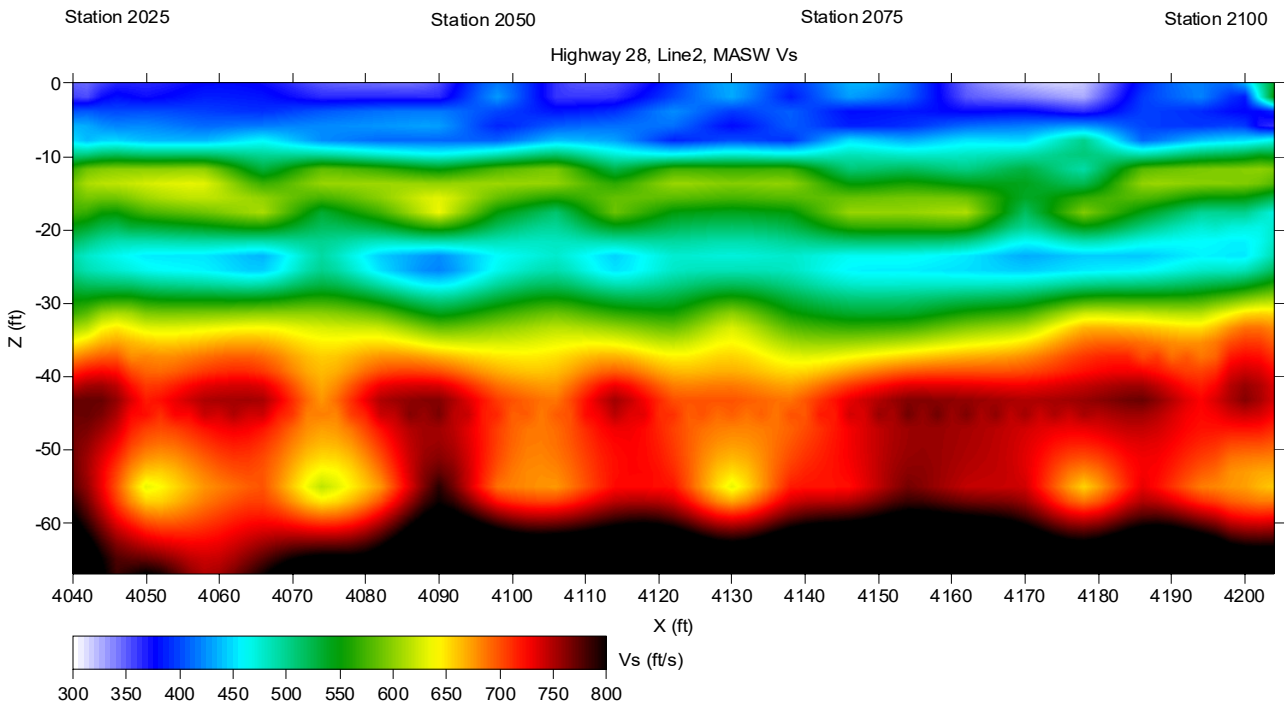

Figure 45. MASW Vs results for Line 2.

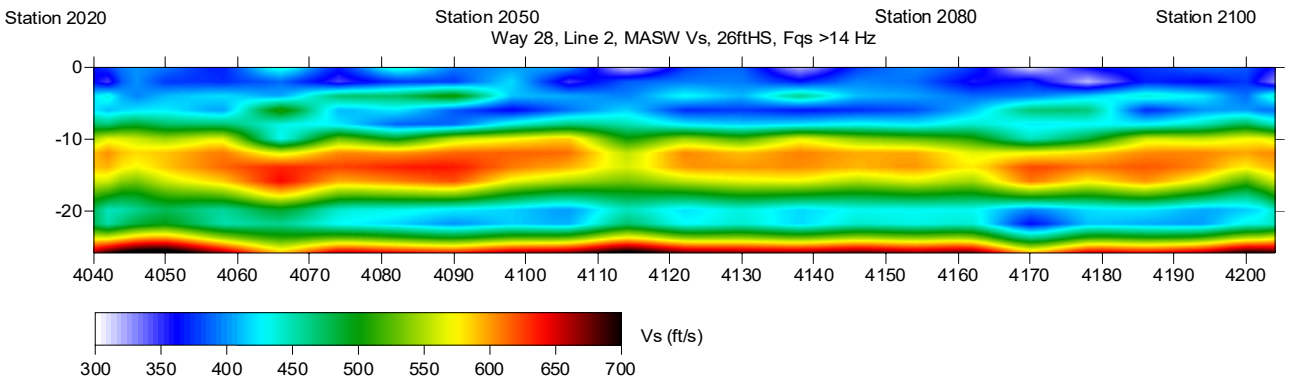

Figure 46. Shallow-focused MASW Vs results for Line 2.

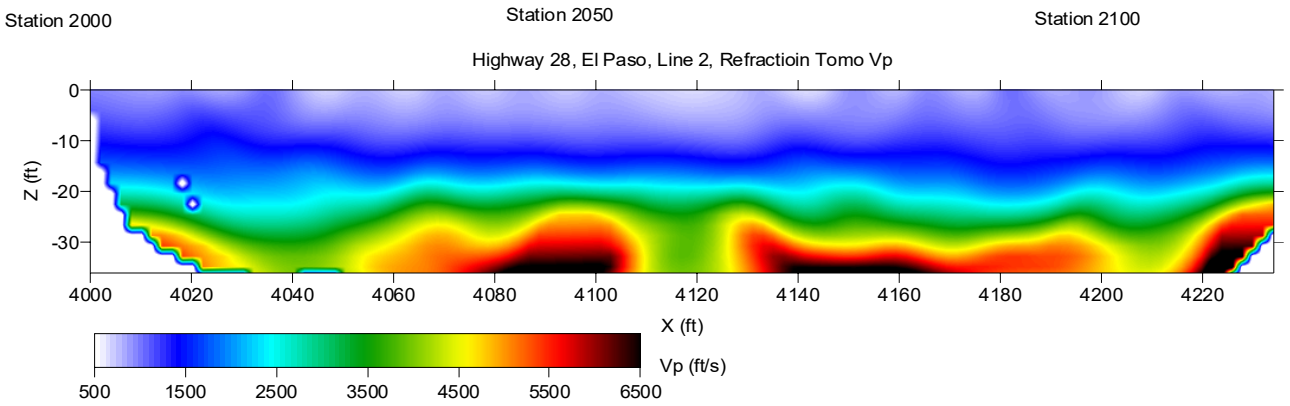

Figure 47. P-wave velocity model estimated for line 2 by analyzing P-wave data first-arrival times using refraction-tomography software.

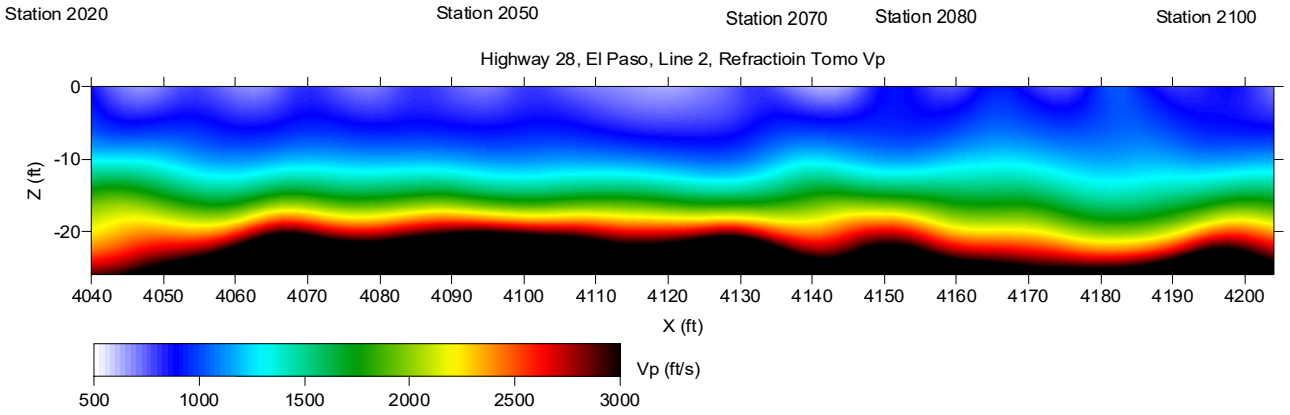

Figure 48. P-wave velocity model estimated for line 2 by analyzing P-wave data first-arrival times using refraction-tomography software rescaled for comparison with the rest of the Vp and Vs results, focusing on the levee.

Traditional MASW processing

Consistent with the processing strategy used on the previous lines, dispersion curves were initially defined based on picks from all possible frequencies (6 to 80 Hz). Inversion results provided a reasonable 2-D Vs image for depth range 2 to 60 ft (Figure 49). This image contributes important general information of the overall structure and to some degree character of the sediments as a function of depth. Unfortunately, these images possessed little detail in the top 10 ft of the section, diagnostic of the internal characteristic of the levees themselves.

Levee-focused MASW processing

Based on the inversion analysis results for lines 1 and 2, the dispersion curves were edited to remove contributions from frequency below 14 Hz, thereby better focusing the MASW result from within the levees. The same shallow inversion model (max 26 ft deep) was used to obtain a 2-D Vs section (Figure 50). Using this approach that proved effective at sites 1 and 2, it was possible to generate a more representative image of the levee.

P-WAVE FIRST ARRIVALS

Characteristics of first-arrivals from line 3 were consistent with the previous two lines and automatically picked from shot gathers, needing very few manual adjustments. The refraction-tomography analysis provided a detailed 2-D Vp solution for line 3 (Figure 51). The 2-D cross section represents a property-specific view or slice of the earth vertically beneath the survey line. This solution was obtained with a minimal number of model iterations and provides an excellent match between the modeled and observed first arrivals. The 2-D Vp solution for line 3 was rescaled to focus on the levee and for ease in comparing with the results of other analysis (Figure 52).

Other Processing

JARS P-WAVE TOMOGRAPHY

The JARS method was developed to overcome the wide range of equally possible solutions for the inverse refraction-tomography problem. It uses a reference compressional-wave velocity (V_p) model, derived from surface-wave shear-wave velocity (V_s) estimates by using an assumption about the V_p / V_s trend (e.g., that the general trend of V_p. follows that of V_s) The JARS method provided more realistic results than other inverse refraction traveltime problem algorithms when applied to seismic data acquired in the Sonora Desert, Arizona, USA (Ivanov et al., 2006). The JARS method was proposed as a superior first-arrival methodology for tomography application along the crest of these levees.

The JARS method was tested with first-arrival data from line 1 (Figure 53). As with any iterative inversion technique, many possible solutions exist for a single data set; the one presented here represents the most likely after considering all *a priori* data. This solution has an RMS error of only 1.29 ms (meaning the data and model are an excellent fit), and therefore represents a very reasonable solution. The JARS V_p solution appears more realistic than the one from conventional refraction-tomography. In addition, the JARS method provides a V_p

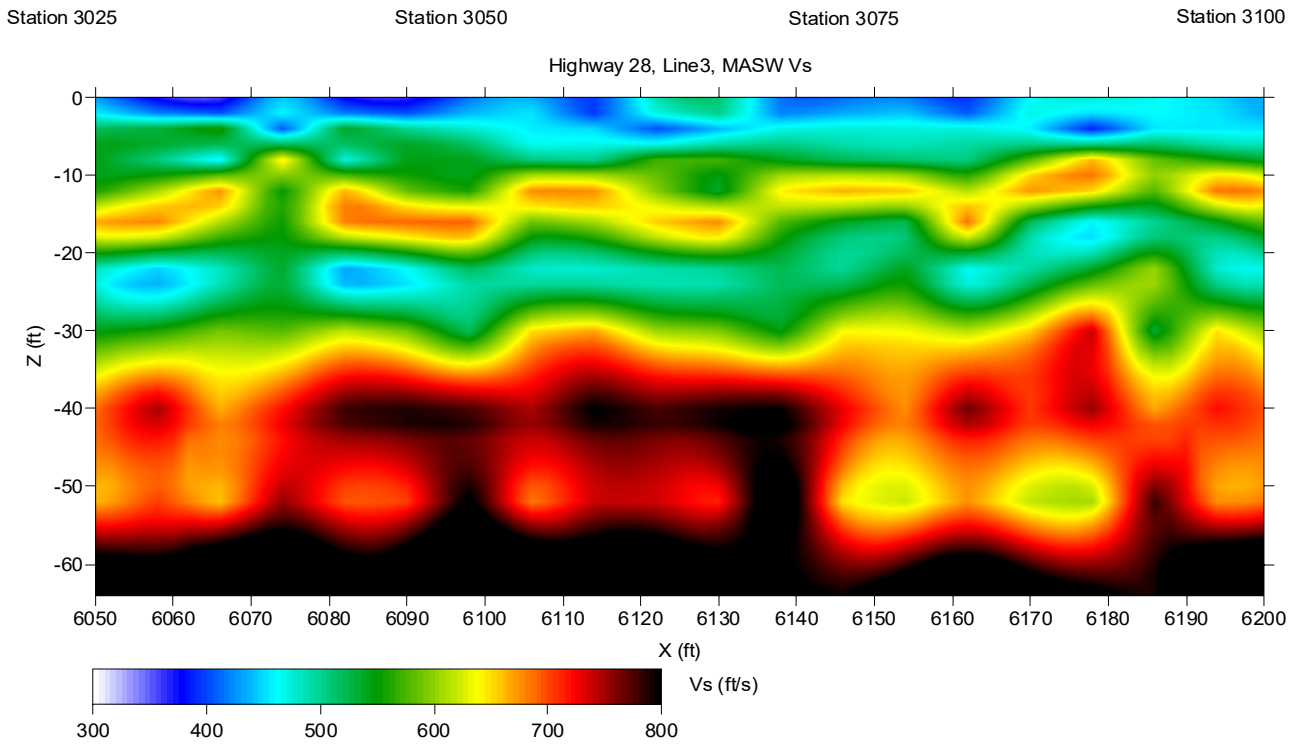

Figure 49. MASW Vs results for Line 3.

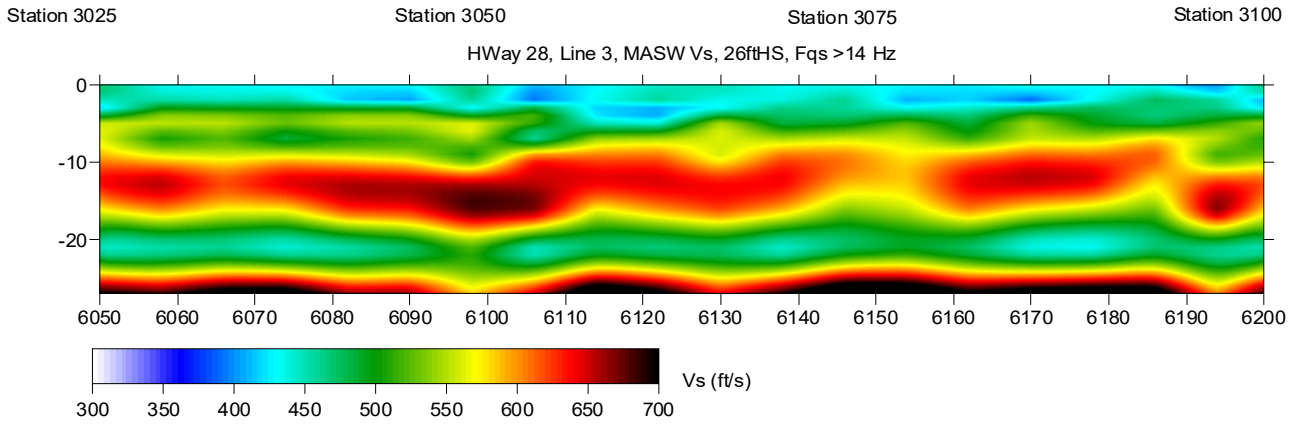

Figure 50. Shallow-focused MASW Vs results for Line 3.

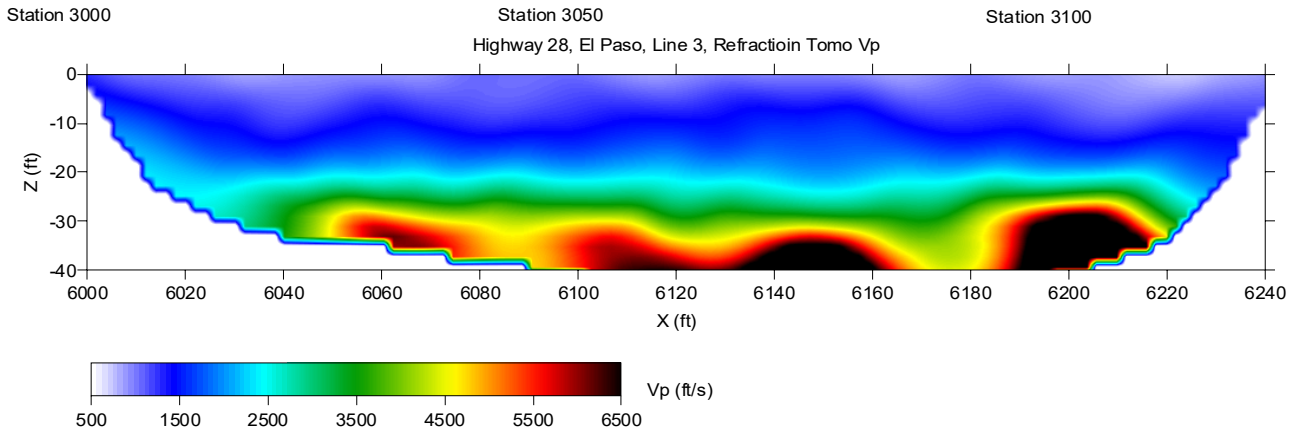

Figure 51. P-wave velocity model estimated for line 2 by analyzing P-wave data first-arrival times using refraction-tomography software.

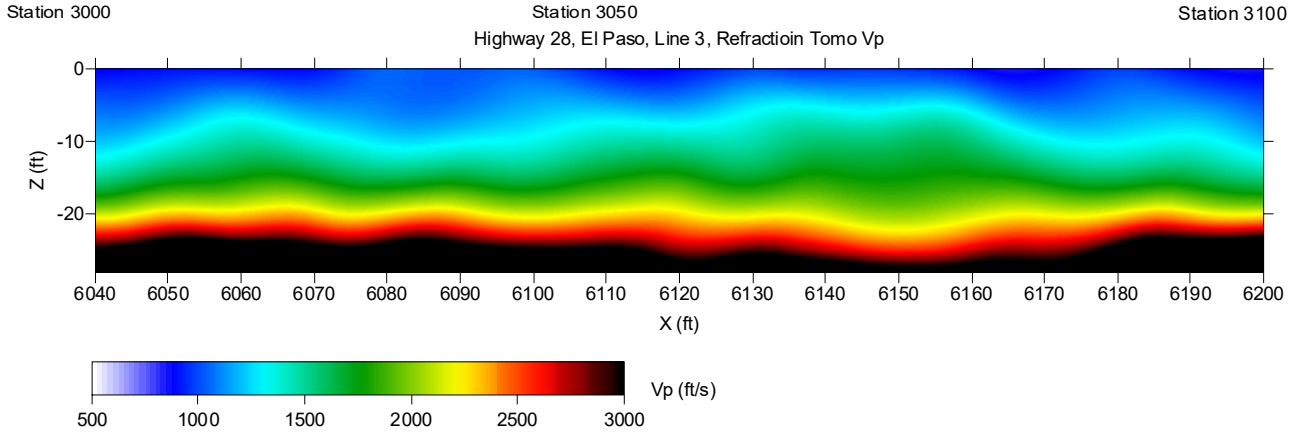

Figure 52. P-wave velocity model estimated for line 2 by analyzing P-wave data first-arrival times using refraction-tomography software rescaled for comparison with the rest of the Vp and Vs results, focusing on the levee.

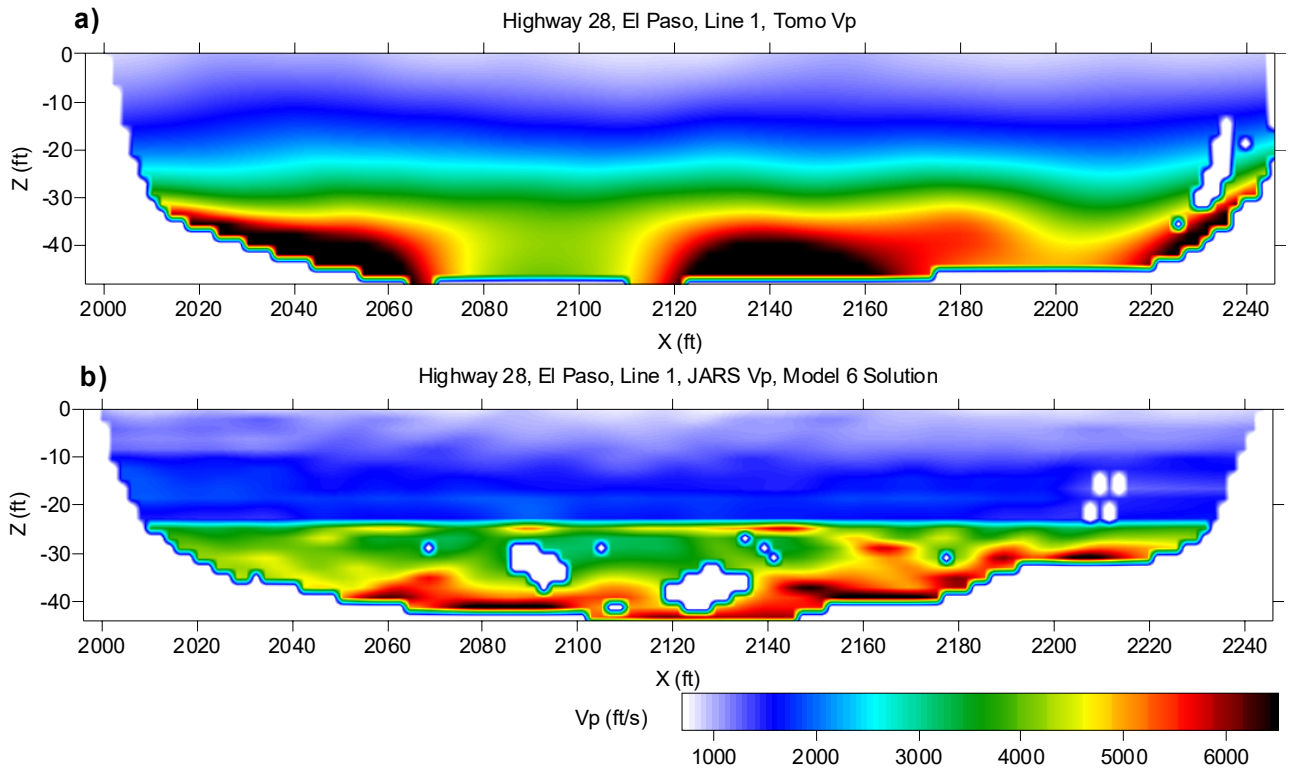

Figure 53. Southern New Mexico 2-D images from P-wave seismic data acquired at the levee crest: a) conventional P-wave refraction-tomography solution, and b) JARS P-wave solution. Blank areas within the images indicate lack of ray coverage and are deliberately left in.

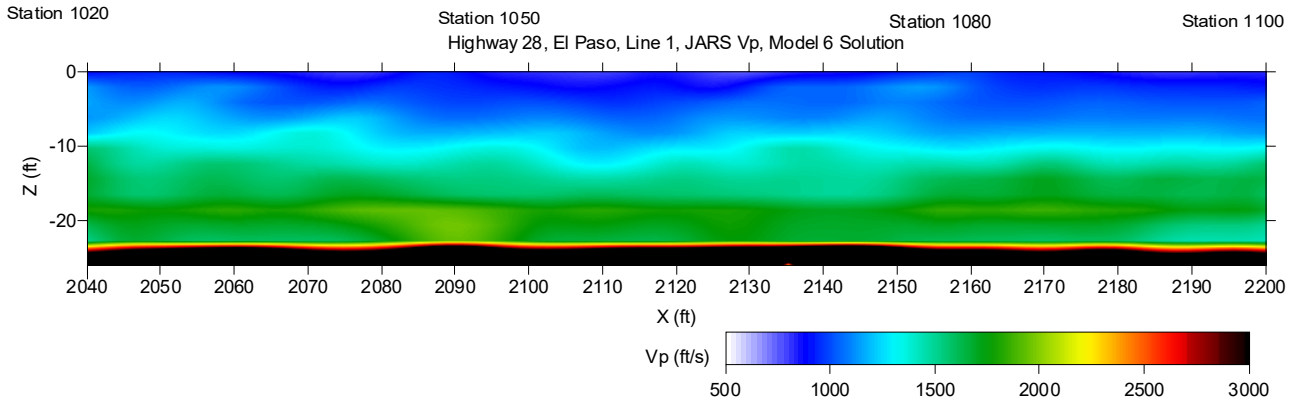

Figure 54. Southern New Mexico 2-D images from P-wave seismic data acquired at the levee crest. JARS P-wave solution focusing on levee-body imaging.

solution that includes a low-velocity layer positioned between high-velocity layers. Such solutions' quality is not offered by any other commercial refraction-tomography algorithm. The 2-D JARS V_p solution for line 1 was rescaled in both dimensions (x and z) to better focus on the levee and for ease of comparison with other results reported on in this document (Figure 54). The JARS imaging of the top part of the section appears more realistic and consistent with the geologic expectations for the site then the refraction-tomography solution (Figure 43).

Observations

The levee body appears as a high Vs anomaly within the depth range 4-8 ft on all 2-D Vs images. Seismic data from lines 2 and 3 provided better fundamental-mode dispersion-curve images when compared to line 1. This difference is likely related to levee homogeneity and corresponding backscatter noise. Such a difference adversely affects the ease with which the MASW method can be used to provide equivalent and therefore comparable side-wide profiles.

The levee image on line 3 appears disturbed between locations 6100-6200 ft. From the pattern observed in the levee image it is possible that this part of the levee at this location is composed of materials mined from a different area thatn the majority of the levee, possible originating from a barrow pit harvesting material near the base of the levee as imaged on this section (Figure 50). A similar high Vp anomaly can be observed at the same location on the corresponding refraction-tomography model of line 3 (Figure 52), which supports the interpretation of anomalous material being the source of the difference relative to the rest of the levee. Of course there are many other possible interpretations but considering the settings this seems most reasonable.

Discussion of Data and Processing of the Ponding Experiment: Trip 2

P-wave First-arrival Analysis

Turning-ray tomography was used to define Vp for subsurface cells between the contact of the levee and native ground surface and the first 40 ft below the basal contact of the levee beneath the crest profile lines (Zhang and Toksoz, 1998).

FIRST-ARRIVAL PICKING

First-arrival seismic energy automatically picked from shot gathers required only minor manual adjustments (Figure 55).

On many shot gathers at source-receiver offsets of ±40 ft the air coupled wave began interfering with first arrivals and as a result error in picking increases and confidence levels dropped. An initial pass at first-arrival picking resulted in refraction-tomography solution that was calculated based on the upfront knowledge that first-arrivals at these longer offset first arrivals were contaminated. Observed and modeled first-arrival times were then examined for inconsistencies with appropriate adjustments made to compensate for those differences.

Large positive (observed first arrivals are greater than the modeled) misfits between 2120 and 2180 (Figure 56) are evident on only two of the shots. One possible explanation was that these misfits were the result of inaccurate first-arrival picks due to noise. Another possibility was these positive misfits are the result of a near-surface velocity anomaly within the levee. First-arrival

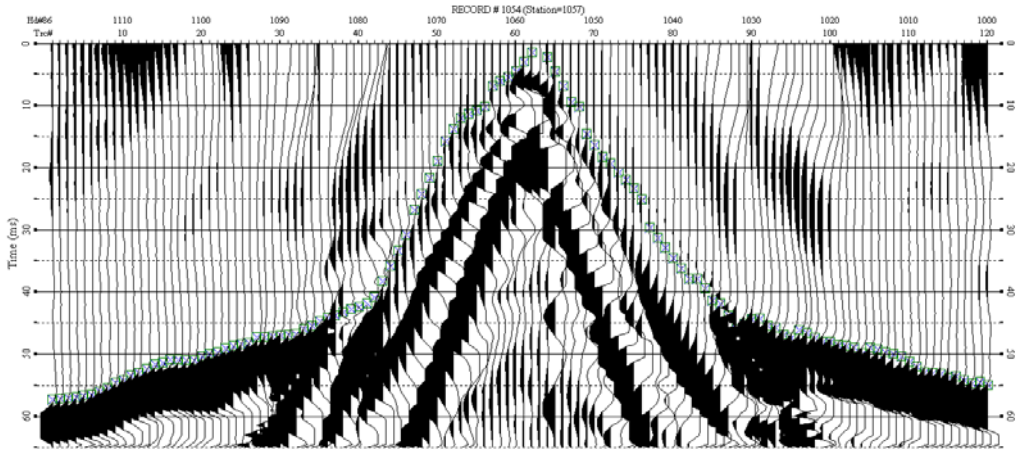

Figure 55. Estimation of first-arrival times on a P-wave seismic data with source located at station 1057 (horizontal location 2114 ft).

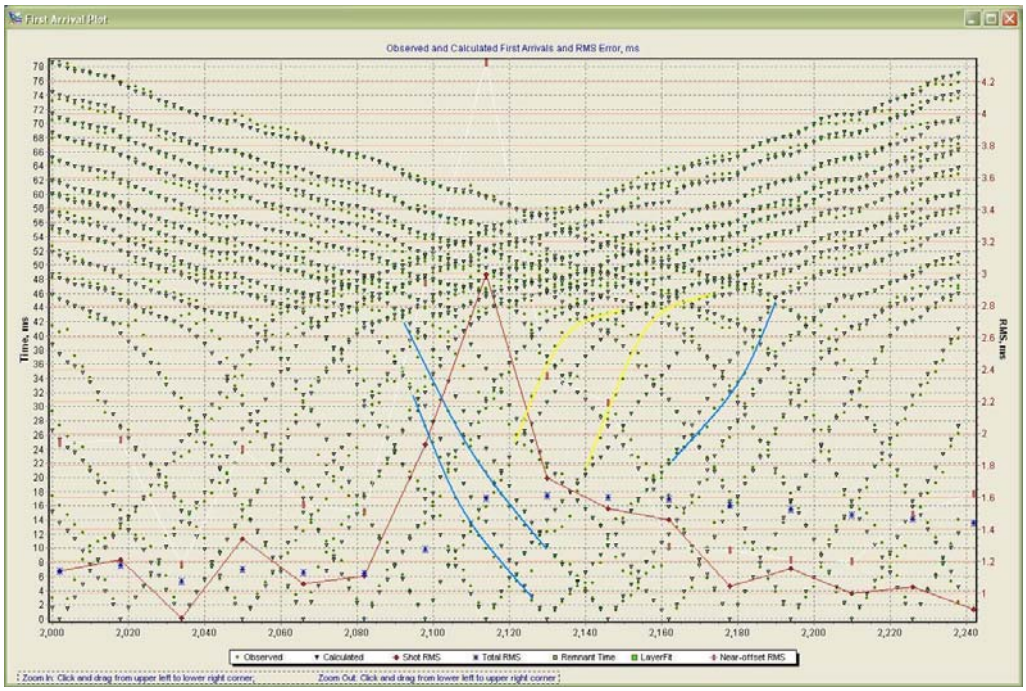

Figure 56. Misfit observations between the modeled (calculated) the observed first arrivals. Yellow lines indicate first arrivals that are greater than the modeled, blue lines indicated those that are smaller.

energy was reexamined again on raw shot gathers and alternative, weak first-arrivals, initially interpreted as noise, were estimated (Figure 57). The newly picked first arrivals matched the calculated first arrivals from the initially estimated velocity model quite well. This approach was then used as a first-pass refraction-tomography solution to distinguish first-arrival patterns due to noise from those due to a true seismic response of the site.

A similar approach was applied on a few of the negative misfits traces between 2090 and 2140.

Further examination of first-arrival misfits on traces within 60 ft of the source revealed that for a single station location within the selection of shots recorded the negative misfits were generally balanced by positive first-arrival misfits of similar degree. This variability predominantly occurs at the transition or cross-over between the first and second layer apparent-velocity slopes. The negative misfits are the result of signal contaminated by the airwave in the transition zone. To minimize the error, this transition zone was deliberately avoided during the analysis, by selecting wavelets immediately after the airwave signature.

The modeling and first-arrival pattern analysis was iterated four times to optimize the solution. Using that approach the influence of ambient noise and airwave on first-arrival analysis was minimized.

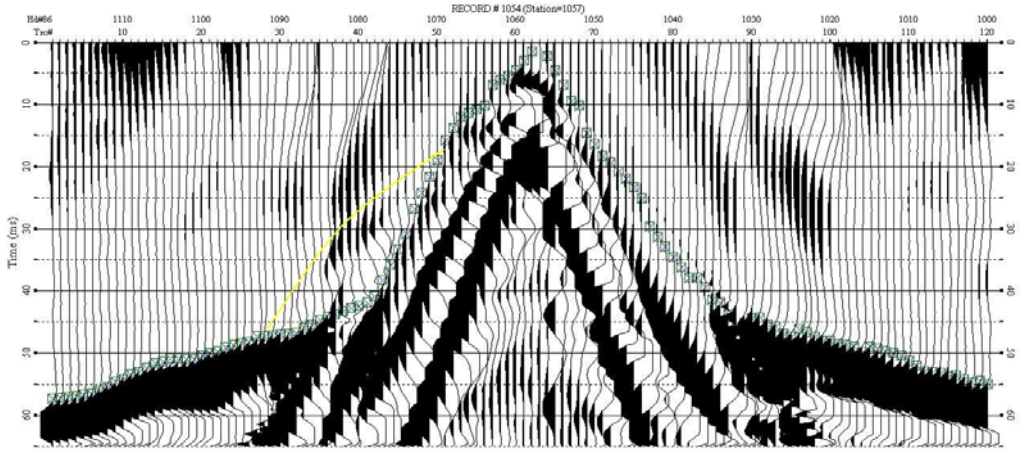

Figure 57. Estimation of first-arrival times on a P-wave seismic data with source located at station 1057 (horizontal location 2114 ft) and the model suggested first arrivals (yellow line).

Choosing Smoothing Parameters and Nonuniqueness

Choosing maximum smoothing constraints is widely accepted as the optimum approach when solving the inverse refraction-tomography problem (as well as any other ill-posed geophysical problem [Constable et al., 1987]). However, smoothing diminishes or eliminates local anomalies. Thus, such an approach may be very harmful when trying to detect or delineate local near-surface anomalies. When investigating levees, detailed delineation of anomalies is, generally, the objective. For this study, the detail necessary for describing the levee is evident in refraction-tomography solutions for line 1 (Figure 58).

One of the main criteria for finding a reasonable or best solution to the inverse refraction-tomography problem is minimizing RMS error between the modeled and observed first-arrivals. In a relative sense, rays that sample the near surface arrive at near offsets, and rays that sample deeper parts of the section arrive at longer offsets. In addition to the traditional RMS estimate, we

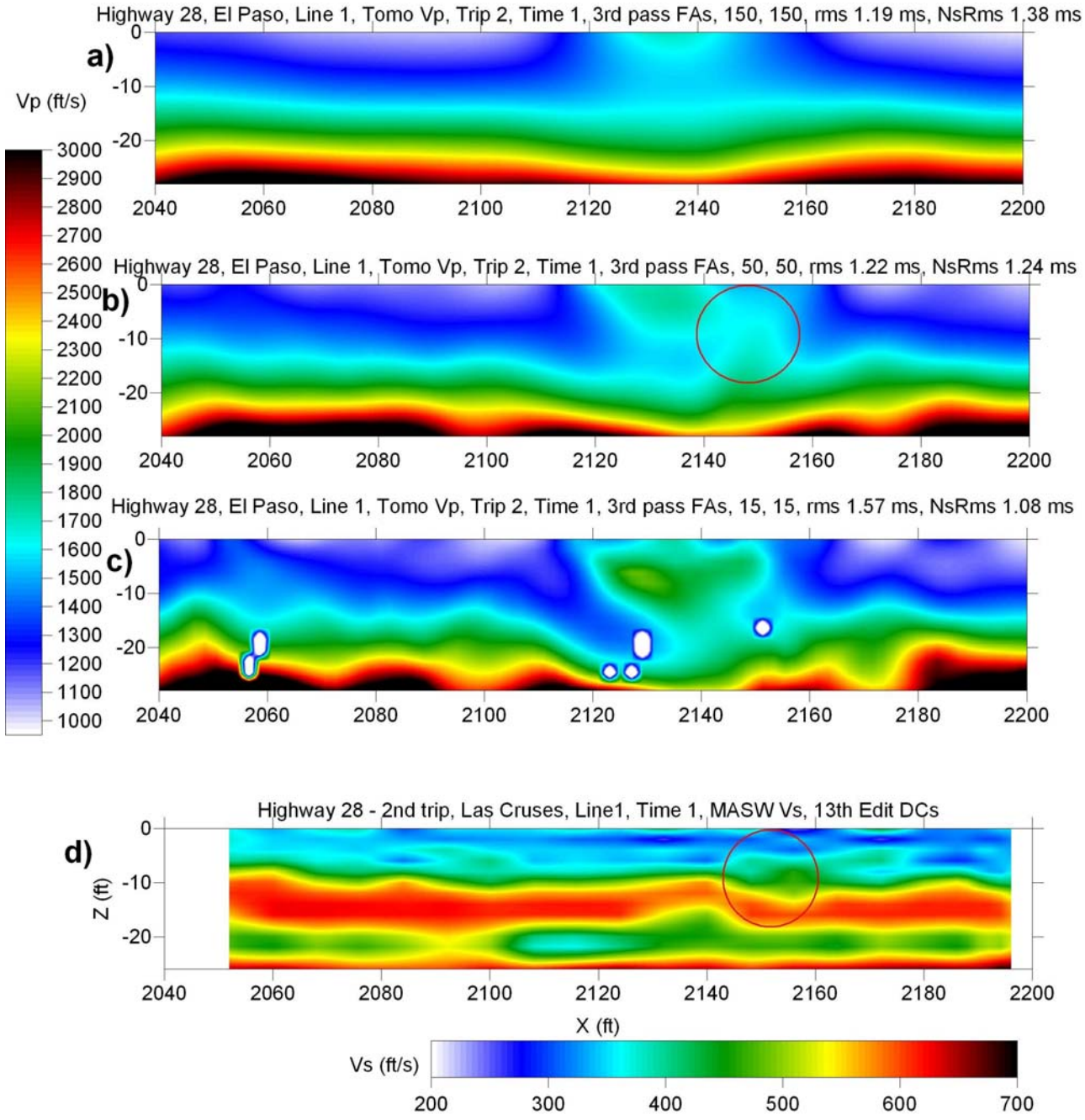

Figure 58. Highway 28, El Paso, Trip 2, Line 1, Vp refraction-tomography inversion regularization parameter (smoothing) testing and comparison with MASW Vs results. Red circles indicate areas with similarities between the Vs and Vp sections.

calculated the RMS fit between the modeled and observed first-arrivals for nearest-offsets, which is one measure of how focused the refraction-tomography analysis is on the near surface.

Selecting regularization parameters (such as smoothing constrains) is considered subjective (Claerboat, 1992, p. 82), regardless of the algorithm used (Tichonov and Arsenin, 1977; Hansen, 1998; Xia et. al., 2005). No matter its forms, smoothing (or any other type of regularization) quantifies expectations (about the solution), which are not based on actual data (Menke, 1989, p. 48). For this data set, we tested several degrees of smoothing, observing both total and near-offset RMS error and evaluating the solutions with the *a priori* information about the site and the MASW results.

We display three refraction-tomography solutions (Figure 58) using different smoothing weights. The weights stabilized the inverse problem by affecting second-order smoothing constraints. The applied weights were 150, 50, and 15 (Figures 58a, 58b, and 58d), in both vertical and horizontal directions. Commercial refraction-tomography algorithms (Rayfract, GeoTomo, Green Mountain, etc.) automatically selected the smoothest solution with a smoothing parameter of 150 or higher (depending on their internal algorithm). This approach may be acceptable when estimating the near-surface model for static corrections but is unsuitable for a levee surveys because high smoothing smears or suppresses local anomalies, which in effect are the principle target of the investigation.

To choose which of the weights provides the most realistic solution we used the Vs section from MASW analysis as additional *a priori* information. The refraction-tomography solution, which used a weight value equal to 50, was selected to maximize resemblance with the Vs section between horizontal locations 2140 and 2160 and depths 8-10 ft (Figure 58b and 58d). The overall RMS error (1.22 ms) was equivalent to the near-offset RMS error (1.24 ms). The weighted (15) refraction-tomography solution (Figure 58c) showed improved near-offset RMS error (1.08 ms), implying a better fit for the near-surface rays paths. However, the overall RMS error was higher (1.57 ms; compared to 1.22 ms) and from a qualitative perspective this solution appeared too irregular to be considered realistic. Rejecting this solution was also supported by the available geologic information, as well as from the MASW Vs images. This sequence of solutions suggests the base of the levee is flat. The maximum-smoothness solution had a low overall RMS error (1.19 ms) but its near-offset RMS error was too large (1.38 ms), indicating poor near-surface representation of the Vp model.

Vp Models During the Ponding Experiment

Using the selected smoothing inversion parameters and first-arrival estimates nine Vp refraction-tomography models were estimated for each time slice during the ponding experiment (Figures 59 and 60).

The baseline survey revealed a high-velocity Vp anomaly between locations 2120 and 2160 ft, an area characterized by a number of animal burrows (Figure 31, top section). This anomaly extended to 10 ft of depth near the start of the flooding experiment and after the first 4 hours could still only be observed within the top 3-4 ft of the levee. Refraction-tomography Vp results for the rest of the line suggests compressional-wave velocity does not appear sensitive to any changes in seismic characteristics of affected levee material that can be attributed to the ponding (Figures 59 and 60). It is also possible that once saturated the clay particles within levee surface or skin sealed and resisted saturation, no material changes took place within the principle imaged zone of the levee.

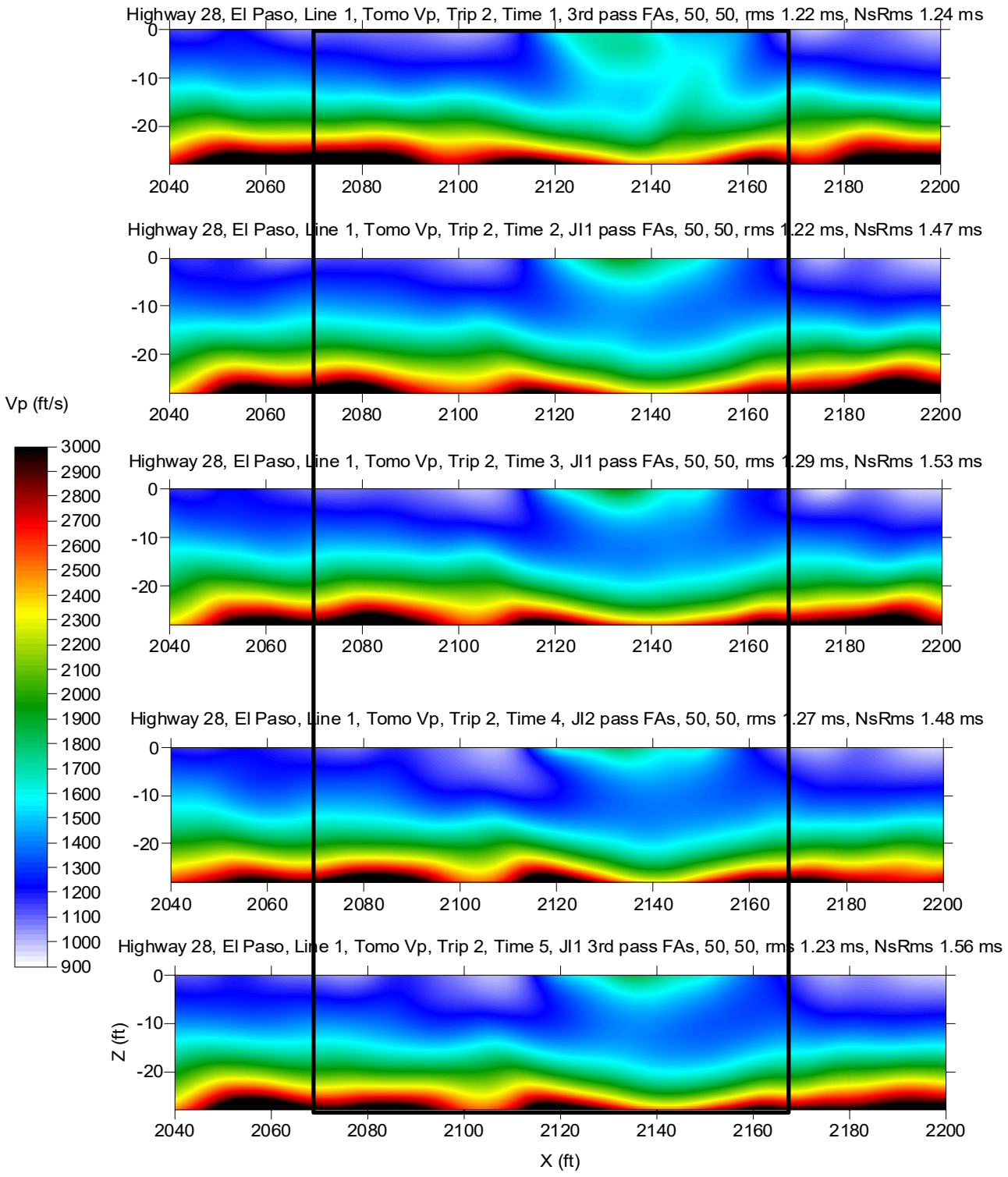

Figure 59. Refraction tomography Vp results at the top of the levee next to the pond for the first five time slices estimated at 4-hour intervals after the beginning of the test with the initial survey at the top and the fifth survey at the bottom of the display. The pond location is indicated by the thick lines.

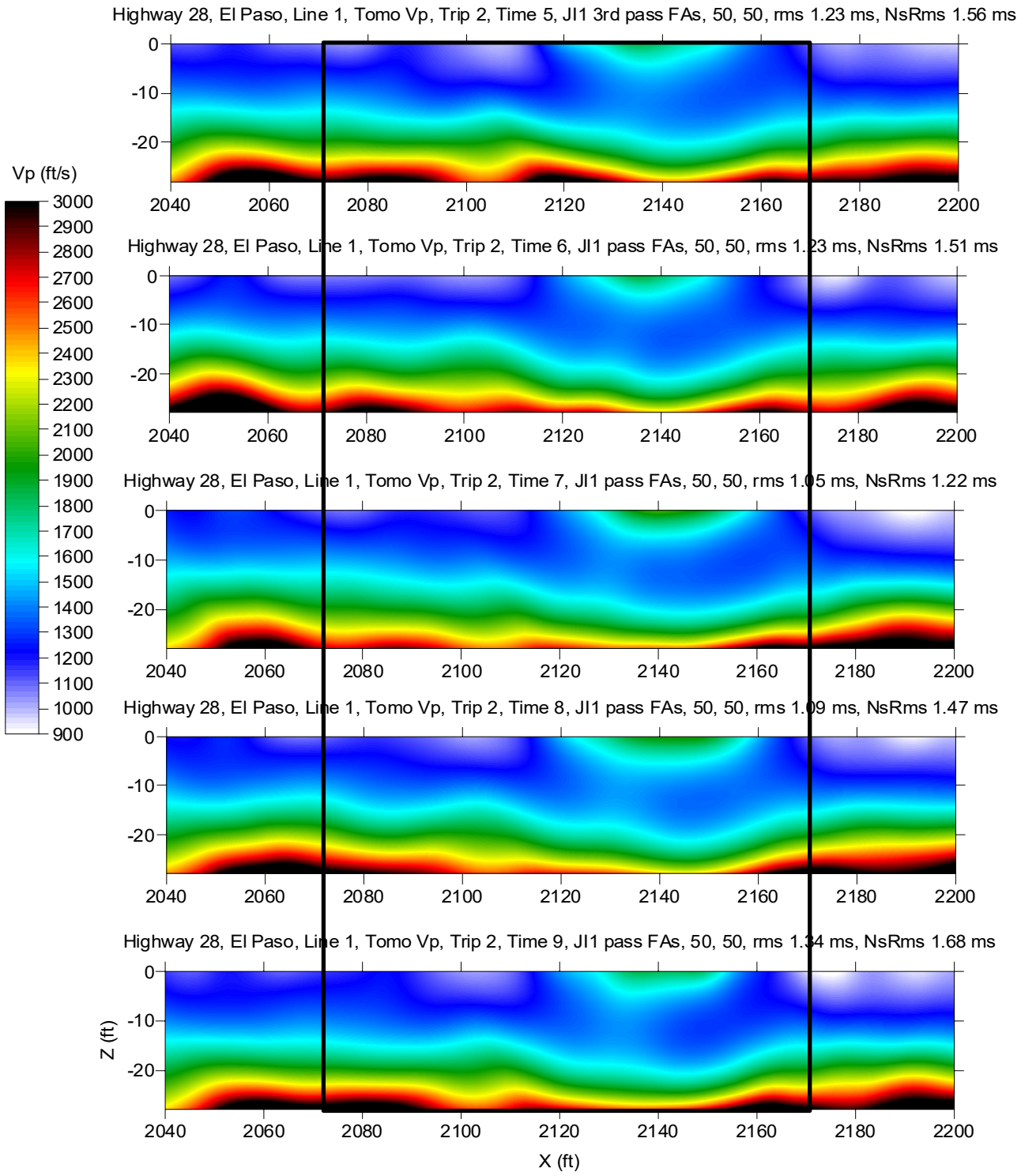

Figure 60. Refraction tomography Vp results at the top of the levee next to the pond for the last five time slices estimated at 4-hour intervals after the beginning of the test with the fifth survey at the top and the ninth survey at the bottom of the display. The pond location is indicated by the thick lines.

MASW

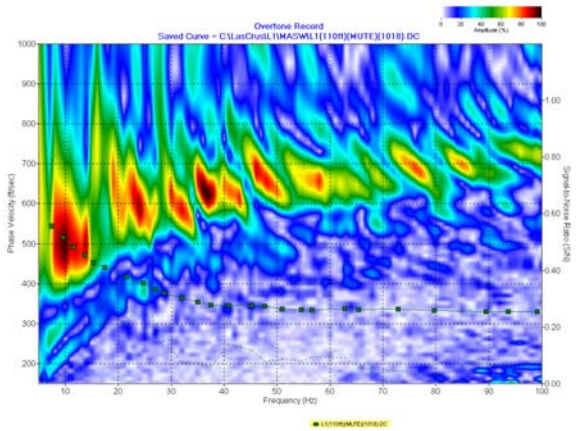

Figure 61. Rayleigh-wave dispersion curve analysis image of phase-velocity versus frequency domain.

The potential of the MASW technique to estimate the dispersion curve of the fundamental mode of the Rayleigh wave from compressional-wave data recorded on the levee crest was demonstrated (Figure 61). The fundamental mode of the surface-wave energy recorded during the time lapse ponding experiment was poorly defined on the second trip to the site compared to the first trip (Figure 29).

At the time of the ponding experiment the fundamental mode of the surface wave was only interpretable within a narrow frequency range between 5-18 Hz and was difficult to estimate at higher frequencies, especially above 30 Hz. As a result, Vs estimates for material within the top 5 ft of the levee possess less confidence and need to be used with caution.

A baseline MASW survey was designed to establish an initial 2-D Vs section and be used as a reference for subsequent time-lapse surveys (Figure 62, top section). Two anomalous high-velocity zones can be observed within the levee body at a depth of about 6 ft between locations 2095 and 2103 ft, and 2145 and 2165 ft. At time slices 2 and 3 (Figure 62, 2nd and 3rd sections from the top), representing 4 and 8 hours after the start of the water fill, the shear-wave properties change and the high-velocity anomalies begin to diminish. As the flooding simulation continues at time slices 3, 4, and 5 (corresponding image numbers from top of Figure 62) the Vs values within the levee continue to decrease to about 10-15% their original values. At the same time a new low-velocity zone begins to form between locations 2098 and 2110 ft at depth greater than 11 ft below the crown of the levee.

This trend continues during time slices 6 and 7 (Figure 63), and by time slices 8 and 9 the low-velocity anomaly is well established and clearly represents a change in the seismic characteristics of the levee and its foundation. Most likely this anomaly relates to ground water movement under the levee. Such water movement could be result in piping making this section of levee susceptible to reduced strength and therefore performance that might not meet design specifications. These anomalies could be catalysts for seepage and therefore threaten levee core integrity, indicative of zones susceptible to failure in extreme cases where the levee is exposed to prolonged high-water conditions. Detection of such anomalies meets one of the objectives of the survey, which is to detect old streambeds running under the levees that could provide conduits for increased ground-water flow thereby indicative of weak spots more prone to failure during flooding.

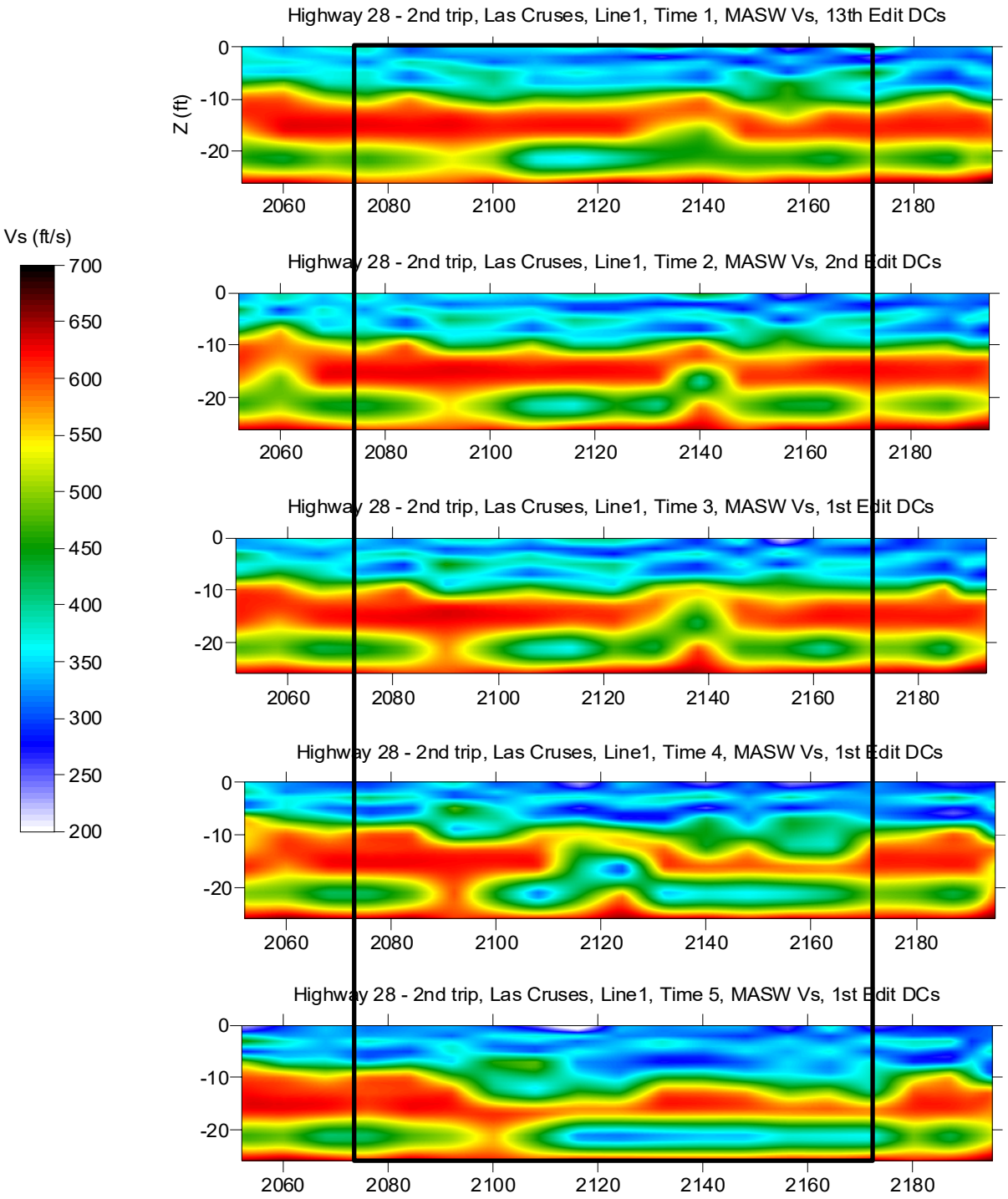

Figure 62. MASW Vs results at the top of the levee next to the pond for the first five time slices estimated at 4-hour intervals after the beginning of the test with the initial survey at the top and the fifth survey at the bottom of the display. The pond location is indicated by the thick lines.

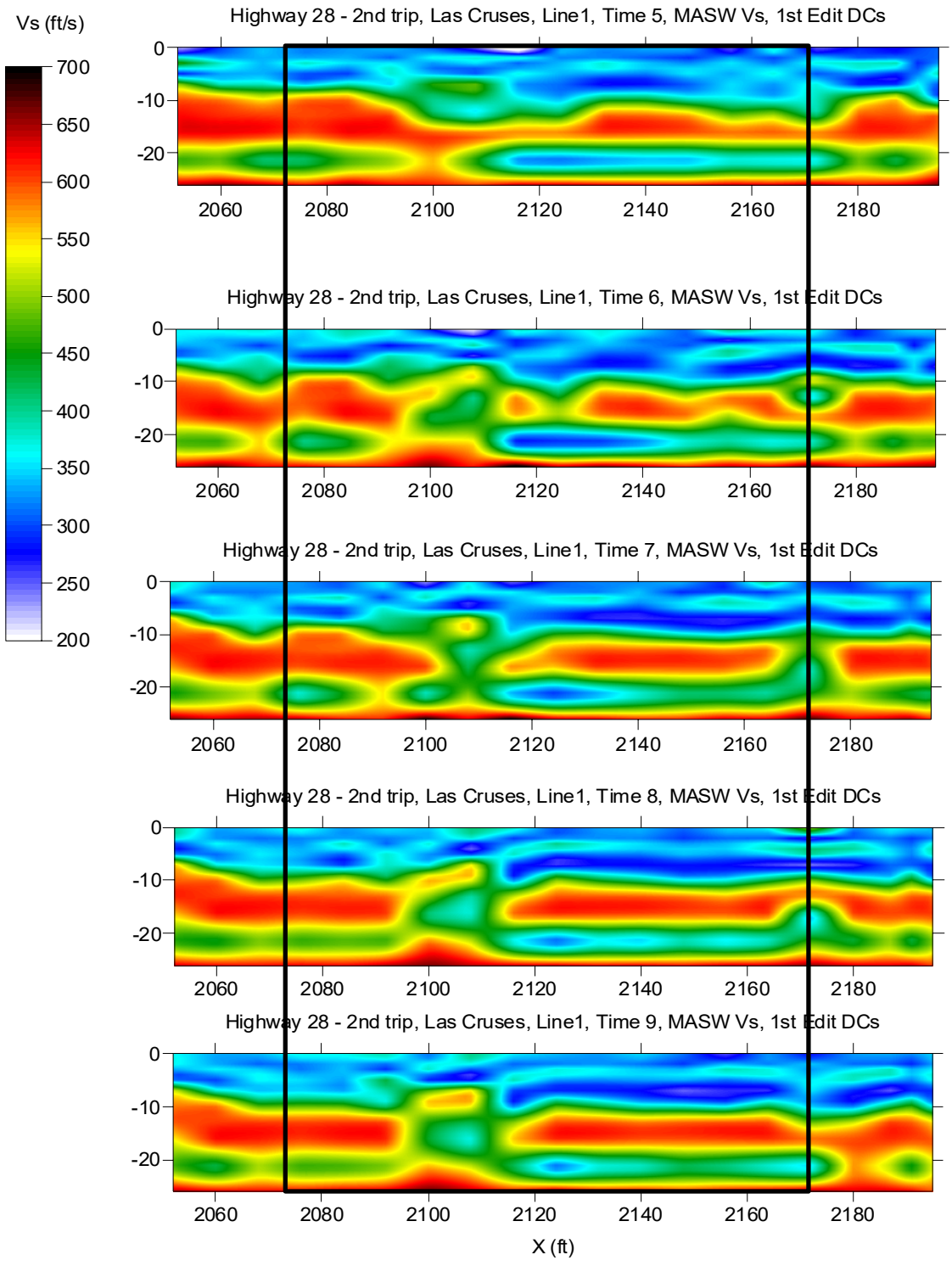

Figure 63. MASW Vs results at the top of the levee next to the pond for the last five time slices estimated at 4-hour intervals after the beginning of the test with the fifth survey at the top and the ninth survey at the bottom of the display. The pond location is indicated by the thick lines.

Discussion

Comparing the Vp and Vs estimates between the two trips shows that, at the time of trip 2, there is a general decrease of Vs (Figure 64) and at least 15% increase of Vp (Figure 65) within the levee (top 10 ft) compared to trip 1. Vp velocity increase between 15 and 20% is evident for most of the top 10 ft, with the exception of the 2110-2160 ft offset range, where the velocity decreases is more than 40%. It is hypothesized that Vp velocity increase is due to higher moisture content in the fine-sand levee shell, a suggestion that is consistent with the rainy period experienced in this area after the first trip (Figure 66).

Therefore, the Vp/Vs ratio (Poisson's ratio) is higher during trip 2 in comparison to trip 1. High Vp/Vs ratio can produce higher amplitude higher modes and weaker fundamental mode (Park, personal communication) as observed during the second trip. This observation is important to the overall understanding and significance of results from MASW surveys. It is relatively easy to estimate the fundamental mode of the surface wave from data acquired during the first trip, while it is very challenging to evaluate it during the second trip.

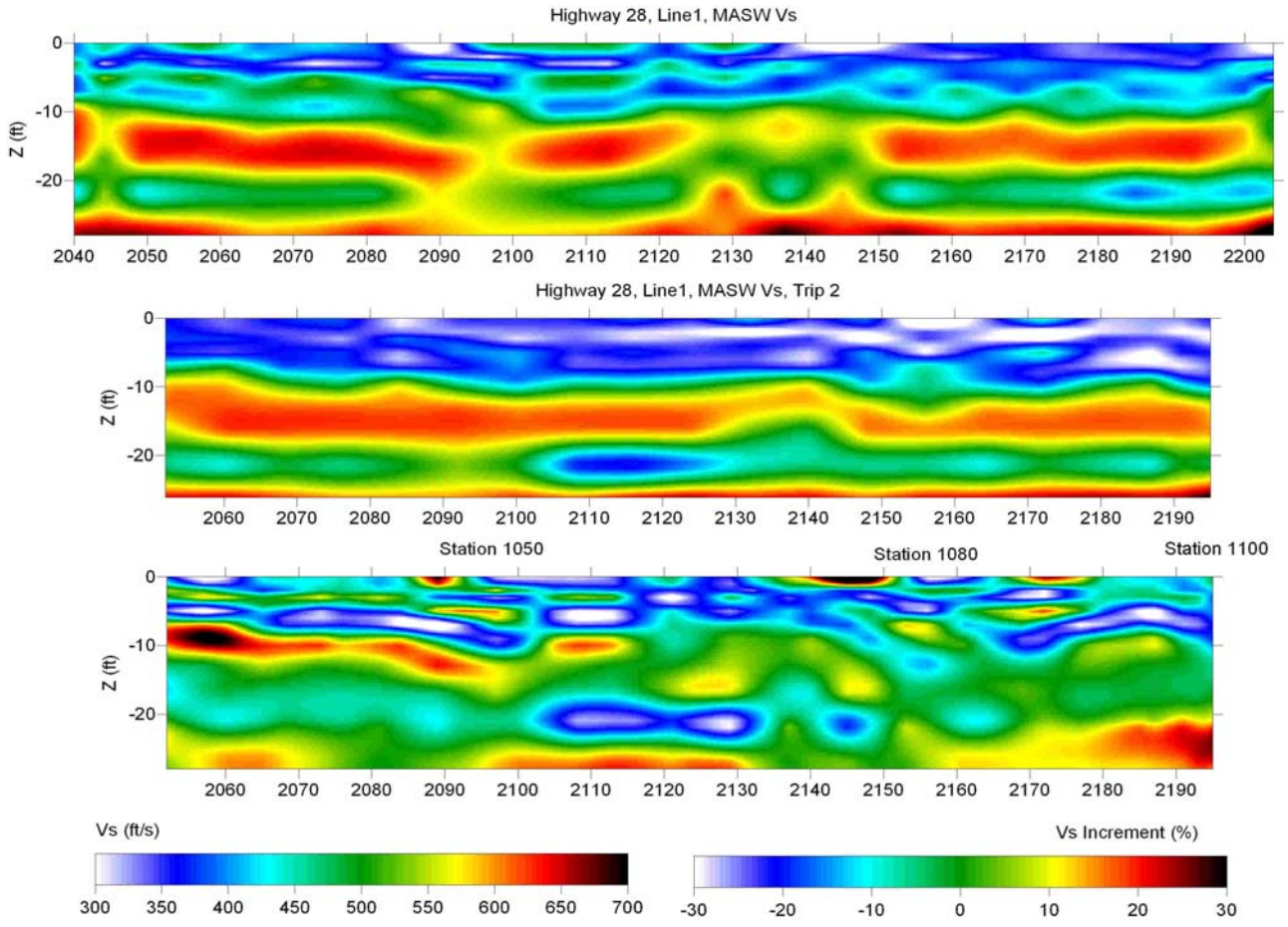

Figure 64. MASW 2-D Vs results for Line 1, a) 2-D Vs model obtained from the seismic data acquired during the first trip, b) 2-D Vs model obtained from the seismic data acquired before the ponding experiment during the second trip, c) difference between the 2-D Vs models obtained in the first and second trips.

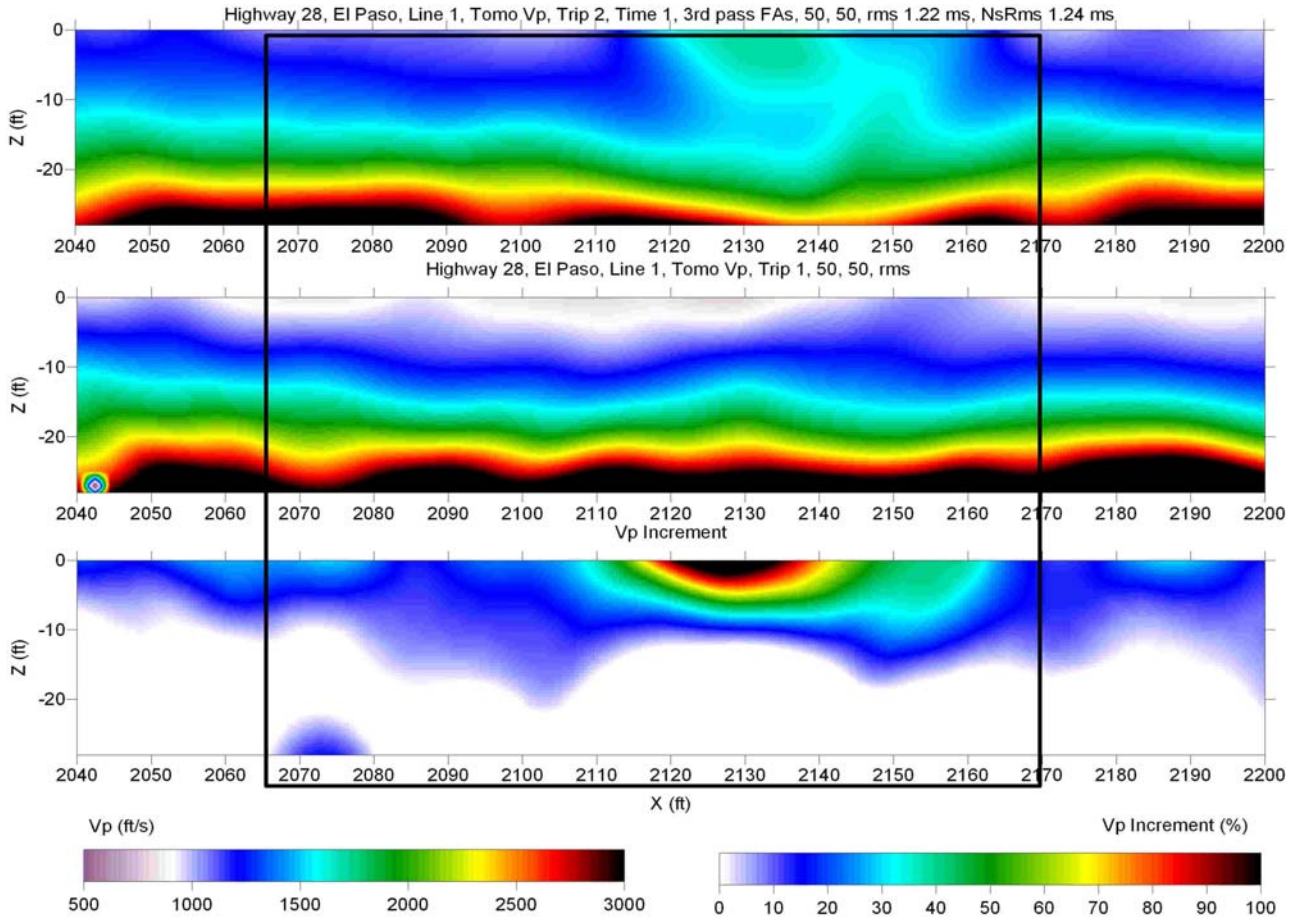

Figure 65. P-wave velocity model estimated for line 1 by analyzing P-wave data first-arrival times using refraction-tomography software, a) P-wave velocity model obtained from the seismic data acquired during the first trip, b) P-wave velocity model obtained from the seismic data acquired before the ponding experiment during the second trip, c) difference between the P-wave velocity models obtained in the first and second trips.

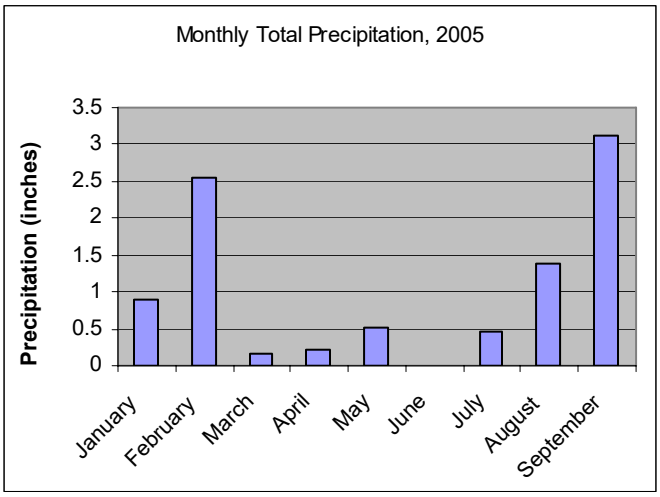

Figure 66. Precipitation measured at State University, New Mexico, in 2005 (Western Digital Climate Center, 2007).

Conclusions

Time-lapse shear-wave profiles calculated from surface-wave energy using the MASW method appear to have changed with increased water depth during the ponding experiment. We assumed these seismic changes are in response to increased saturation below the levee as water infiltrated the foundation during the flood simulation. No noticeable changes occurred in the compressional-wave properties within the levee except for a small volume speculated to be compromised by animal burrows. Vs was the measured material property most significantly affected from increased saturation driven by the hydraulic head provided by the water in the pond.

In general, both compressional- and shear-wave velocity estimates for this type of fine-sand levee suggest increased fluid due to a high water stand against the levee might lead to increased Vp and decreased Vs values and thus decrease levee strength.

SUPPLEMENTAL RESEARCH

P-wave Reflection Seismic at the Toe on the River Side of the Pond

The objective of the experiment was to monitor change in the shallow water table caused by changes in seismic reflectivity directly related to density or velocity with increased sediment saturation. Since this single CMP profile line was acquired multiple times, it was of interest to determine what effect, if any, the source had on the results. Specifically, change in source signature may account for variation between time-lapse survey, which in turn could be misinterpreted as an effect of material change rather than source pulse changes.

A seismic reflection line run parallel to the levee in the floodplain between the river and the dam was located approximately 20 feet from the base of the dam and extended nearly its entire length. Two 40 Hz geophones separated by 1 foot were used at each station to record the data. There were 2000 samples per trace with a 0.25 ms sample interval. The source was a 30.06 fired downhole; source spacing was 8 feet. A baseline survey was shot first, after which water was pumped into the pond for 4 hours.

SEISMIC REFLECTION PROCESSING

The first run was processed using the procedure described below; the remaining 8 runs were processed the same, except for velocity analysis. Normal move-out was corrected for each run individually.

Automatic gain control (AGC) with a 20 ms window was applied to balance the amplitude of energy arrivals through time on raw data. The field geometry was then assigned. The data were filtered with a 100 to 500 Hz bandpass filter. Bad traces were muted. Static corrections were then made based upon GPS elevation data.

First arrivals, surface waves, and air waves were filtered using a filter in the frequency-wave number domain (f-k). This technique was successful at suppressing the air waves and enhancing signal, with the portion of the air-coupled wave that remained surgically muted along with everything except confidently identifiable signal. The data were then resorted into CMPs. Velocity analysis was done, the data were corrected for normal move-out, and stacked to produce a final stacked section.

Note that spectral balancing and spherical divergence corrections were both attempted. Spectral balancing greatly decreased the amplitude of the data, unacceptably decreasing the signal to noise ratio. Correcting for spherical divergence made no obvious difference in the quality of the data. Therefore, neither of these processing techniques were used in the production of the final stacked sections.

After processing, the data were reprocessed using the procedure described above, except for the AGC. This was done to preserve true amplitudes for analytical purposes.

SEISMIC REFLECTION ANALYSIS

Immediately obvious during processing was the overall relative amplitude of the air-coupled wave. Qualitatively, its strength appeared to decrease after the survey relative to the second, then strengthen throughout the remaining runs. To analyze its relative amplitude as a function of time, everything except the air wave was muted from the shot gathers following application of the bandpass filter. Frequency spectra were defined for each shot gather of each run. There were several different peak frequencies in the air wave spectra. The true amplitudes of these peak frequencies were recorded from each frequency spectra. The average amplitude of each frequency component was calculated for each run and plotted as a function of time. The average amplitude of the air wave was determined by averaging the mean amplitude of each frequency for each run and plotting it as a function of time (Figure 67).

After undesired data were surgically muted the remaining signal and noise were analyzed in the same fashion as the air wave (Figure 68).

To understand how reflection strengths changed, the same trace in the same shot gather was analyzed for each run. Everything except the desired reflection was surgically muted from the first four shot gathers, and a frequency spectrum for each of these shot gather was generated. The peak frequency and its amplitude were recorded, and two plots were generated for each shot gather: the reflection frequency vs. time, and reflection amplitude vs. time. This was done for the reflections at approximately 35.8 ms and 55.0 ms. The reflection frequency did not change significantly or with any sort of pattern. The reflection amplitudes vs. time can be seen for the 55.0 ms reflection (Figure 68).

To evaluate how the source signature changed with repeat shots, a single trace from the same shot gather during each run was selected and the correlation coefficient was determined for each of the nine wavelets, first correlated with the first wavelet, then with the second wavelet. This was repeated for 5 traces, both near and far relative to the source. Plots of correlation coefficient vs. time were generated for each (Figures 69 and 70).

ANALYSIS OF THE RESULTS

Note the distinct drop in amplitude from 14,064.29 units to 5784.217 between runs 1 and 2, a decrease of almost 60% (Figure 67). After this initial drop in amplitude the average amplitude increases nearly linearly throughout the remaining runs. This drop in air-wave amplitude evident between the first two runs turns out to be very significant. This shows the improvement in source coupling to the ground after firing the gun downhole just once. Source coupling then linearly increases throughout the remaining seven runs. This suggests that to optimize data acquisition in this setting using a 30.06 or similar source, one should fire a shot downhole at least once before

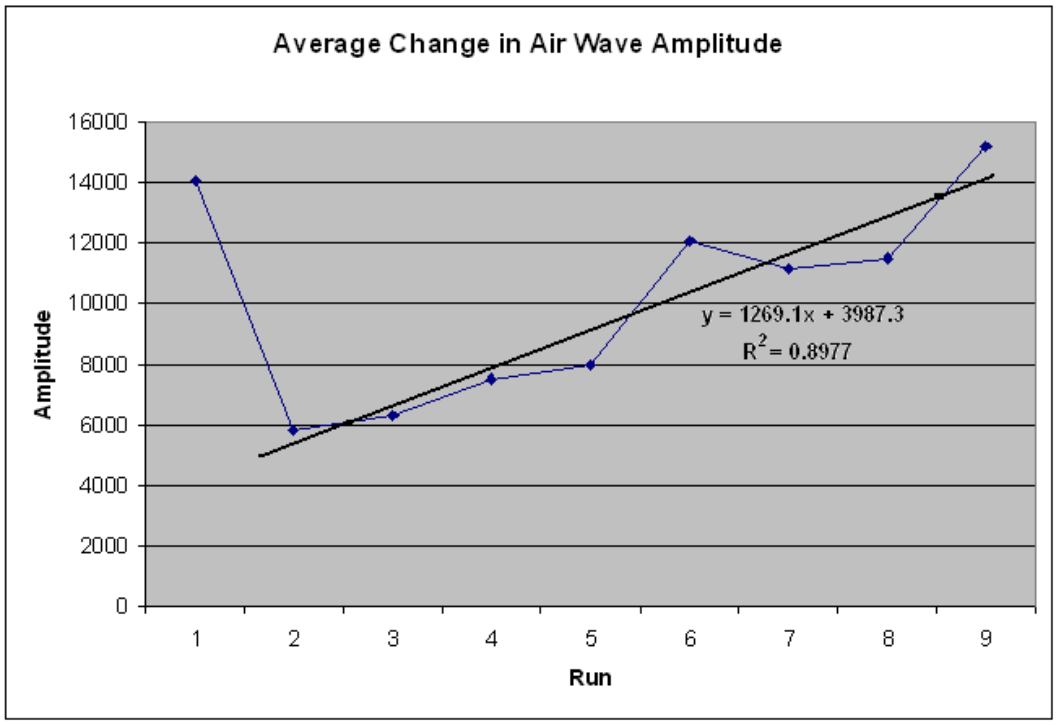

Figure 67. Average change in airwave amplitude.

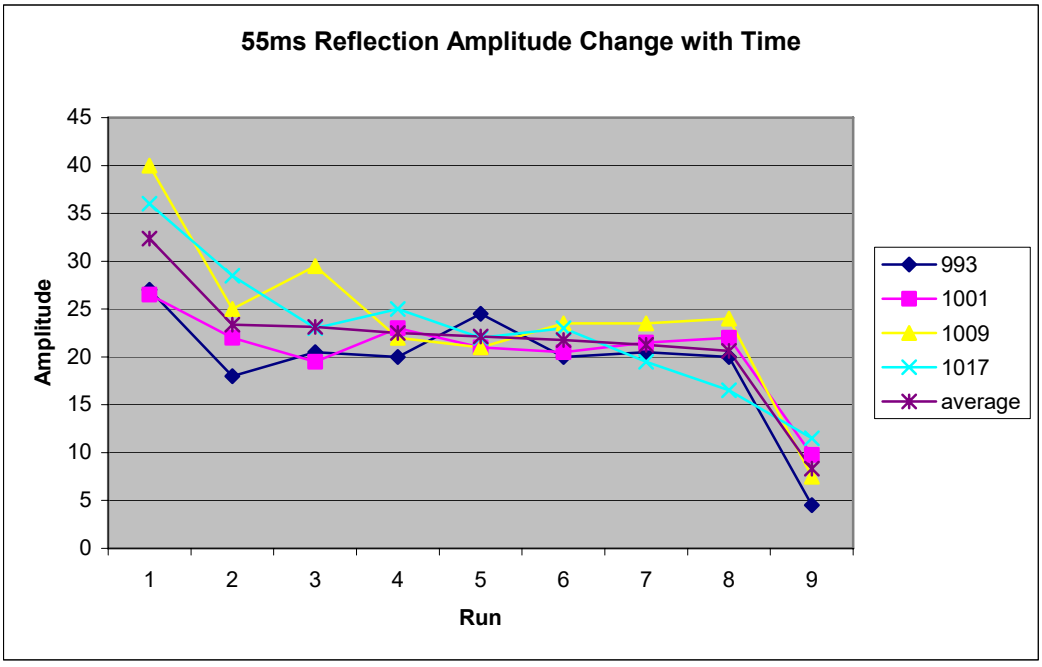

Figure 68. Change in reflection amplitude with time for the 55.0 ms reflection at the first four source stations.

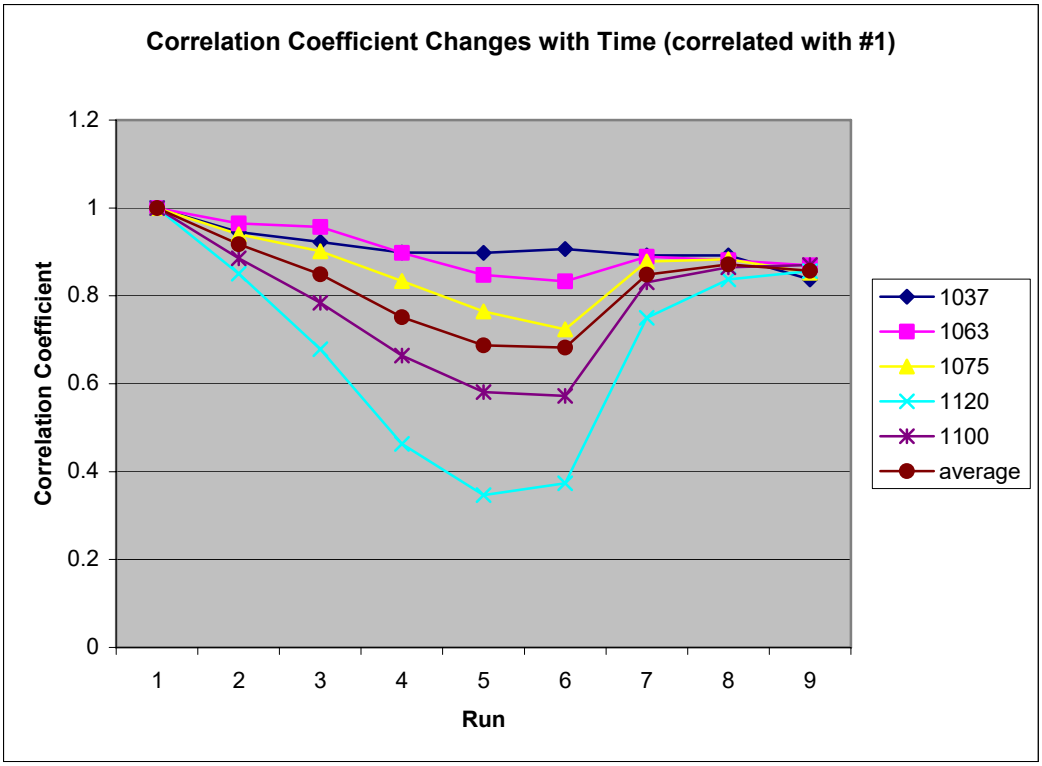

Figure 69. Correlation coefficient for wavelets correlated with that of run 1 for each run. These wavelets were taken from the same shot location, CMP 1017.

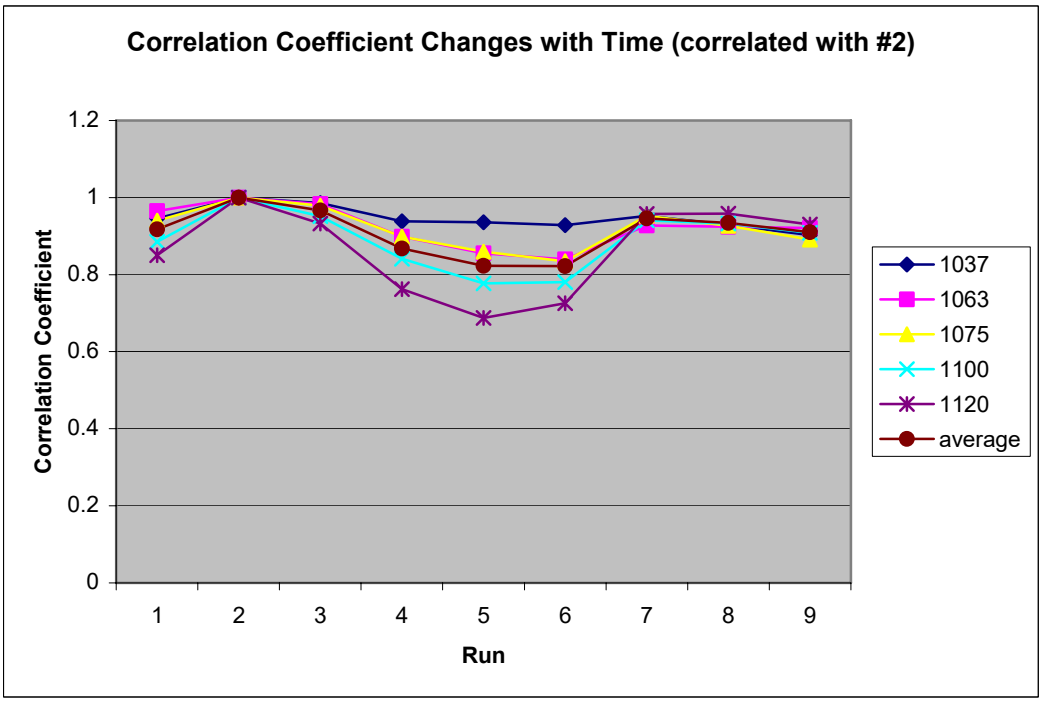

Figure 70. Same as Figure 69, except correlated with the wavelet from run 2, as opposed to 1.

acquiring any data. This will provide increased source coupling on successive shots. No more than eight shots can be fired before source coupling degrades to what it was at the first initial shot.

Reflection amplitude drops between the first and second run, followed by a steady recorded amplitude until it drops again between runs 8 and 9 (Figure 68). The first drop averages 38%. The second major drop averages 60%. Note that these amplitudes are much smaller than those observed for the air wave. This seems to indicate a level of consistency between runs 2 through 8, while there is a distinct change after 1 and before 9. Consistent with air-wave data, reflection amplitudes seem to indicate optimal data acquisition is experienced between runs 2 through 8 (though for different reasons).

There are three things to note about Figures 69 and 70. First, the wavelets from other runs correlate much better with the wavelet from run two (Figure 70) than run one (Figure 69). Second, in general, the farther the geophone is from the source, the smaller the correlation coefficient. Third, the coefficients decrease through run 5, and then unexpectedly increase for the remaining runs.

The fact that the second run correlates better with successive runs than the first run indicates that there was a dramatic change in the source signature after the gun was fired downhole just once. Source signature does continue to change, but it is much more similar to the second run than the first.

It makes sense that the farther the geophone is from the source, the correlation is not quite as good. The energy has been transported farther and had more opportunity to vary due to variable attenuation related to subtle changes in material properties and depositional character.

The decrease in correlation coefficient with run is expected because of the change in source signature from shot hole degradation and internal (inside shot hole) compaction of the surrounding unconsolidated sediments. This should be expected throughout the nine runs. However, there is a slight increase at run 6 and a significant increase at run 7. This does not correspond to any other significant change at run 7. Therefore, there was some change that occurred that did not significantly affect any reflection or air-wave amplitudes and/or frequencies or seismic velocities.

References

Batzle, M., D. Han, and J. Castagna, 1999, Fluids and frequency dependent seismic velocity of rocks [Exp. Abs.]: Soc. Explor. Geophys., p. 5-8.

Berryman, J.G., P.A. Berge, and B.P. Bonner, 1999, Role of λ-diagrams in estimating prorosity and saturation from seismic velocities [Exp. Abs.]: Soc. Explor. Geophys., p. 176-179.

Claerboat, J.F., 1992, Earth sounding analysis: processing versus inversion: Blackwell Science Publications.

Clement, W.P., S. Cardimona, A.L. Endres, and K. Kadinsky-Cade, 1997, Site characterization at the Groundwater Remediation Field Laboratory: *Leading Edge*, v. 16, p. 1617-1621.

Chiu, S.K.L., E.R. Kanasewich, and S. Phadke, 1986, Three-dimensional determination of structure and velocity by seismic tomography: *Geophysics*, v. 51, p. 1559-1571.

Coffeen, J.A., 1978, *Seismic Exploration Fundamentals*: PennWell Publishing Company, Tulsa, OK, 277 p.

Constable, S.C., R.L. Parker, and C.G. Constable, 1987, Occam's inversion: A practical algorithm for generating smooth models from electromagnetic sounding data: *Geophysics*, v. 52, p. 289-300.

Cottin, J.F., P. Deletie, H. Jacquet-Francillon, J. Lakshmanan, Y. Lemoine, and M. Sanchez, 1986, Curved ray seismic tomography–Application to the Grand Etang Dam (Reunion Island): *First Break*, v. 4, no. 7, p. 25-30.

Dobrin, M.B., and C.H. Savit, 1988, *Introduction to Geophysical Prospecting*: McGraw-Hill Book Co., New York.

Glover, R.H., 1959, Techniques used in interpreting seismic data in Kansas: In Symposium on Geophysics in Kansas, ed. W.W. Hambleton. Kansas Geological Survey Bulletin 137, p. 225-240.

Goforth, T., and C. Hayward, 1992, Seismic reflection investigations of a bedrock surface buried under alluvium: *Geophysics*, v. 57, p. 1217-1227.

Guo, T., and L. Liu, 1999, Non-intrusive evaluation of submarine tunnel foundation using dynamic high-frequency surface wave prospecting: Proceedings of the Symposium on the Application of Geophysics to Engineering and Environmental Problems (SAGEEP 1999), Oakland, Calif., March 14-18, p. 67-74.

Haeni, F.P., 1978, Computer modeling of ground-water availability in the Pootatuck River valley, Newtown, Connecticut, with a section on quality of water by Elinor H. Handman: U.S. Geological Survey Water Resources Investigations Open-file Report 83-4221.

Haeni, F.P., 1986, Application of continuous seismic reflection methods to hydrologic studies: *Ground Water*, v. 24, p. 23-31.

Hansen, C., 1998, Rank-deficient and discrete ill-posed problems. Numerical aspects of linear inversion: Department of Mathematical Modeling, Technical University of Denmark, Lyngby.

Hunter, J.A., S.E. Pullan, R.A. Burns, R.M. Gagne, and R.L. Good, 1984, Shallow seismic reflection mapping of the overburden-bedrock interface with the engineering seismograph–Some simple techniques: *Geophysics*, v. 49, p.1381-1385.

Ivanov, J.M., C.B. Park, R.D. Miller, and J. Xia, 2000, Mapping Poisson's ratio of unconsolidated materials from a joint analysis of surface-wave and refraction events: Proceedings of the Symposium on the Application of Geophysics to Engineering and Environmental Problems (SAGEEP 2000), Arlington, Va., February 20-24.

Ivanov, J., R.D. Miller, J. Xia, and D.W. Steeples, 2005a, The inverse problem of refraction traveltimes, part II: Quantifying refraction nonuniqueness using a three-layer model: *Pure and Applied Geophysics*, v. 162, n. 3, p. 461-477.

Ivanov, J., C.B. Park, R.D. Miller, and J. Xia, 2005b, Analyzing and filtering surface-wave energy by muting shot gathers: *Journal of Environmental and Engineering Geophysics*, v. 10, p. 307-321.

Ivanov, J., Miller, R.D., Xia, J., Steeples, D., and Park, C.B., 2006, Joint Analysis of Refractions with Surface Waves: An Inverse Refraction-Traveltime Solution: *Geophysics*, v. 71, p. R131-R138.

Jongerius, P., and K. Helbig, 1988, Onshore high-resolution seismic profiling applied to sedimentology: *Geophysics*, v. 53, p. 1276-1283.

Kilty, K.T., and A.L. Lange, 1990, Acoustic tomography in shallow geophysical exploration using a transform reconstruction: Soc. Explor. Geophys. Investigations in Geophysics no. 5, S.H. Ward, ed., *Volume 3: Geotechnical*, p. 23-35.

Knapp, R.W., and D.W. Steeples, 1986, High-resolution common-depth-point, seismic-reflection profiling: Field acquisition parameter design: *Geophysics*, v. 51, p. 283-294.

Lankston, R.W., 1990, High-resolution refraction seismic data acquisition and interpretation: Soc. Explor. Geophys. Investigations in Geophysics no. 5, Stan H. Ward, ed., *Volume 1: Review and Tutorial*, p. 45-73.

Lanz, E., H.R. Maurer, and A.G. Green, 1998, Refraction tomography over a buried waste disposal site: *Geophysics*, v. 63, p. 1414-1433.

Lytle, R.J., and K.A. Dines, 1980, Iterative ray tracing between boreholes for underground image reconstruction: *Inst. Electr. Electron. Eng. Trans. Geosci. Remote Sensing*, v. GE-18, p. 234-240.

Menke, W., 1989, *Geophysical Data Analysis: Discrete Inverse Theory*: Academic Press, Inc.

Michaels, P., 1999, Use of engineering geophysics in the design of highway passing lanes: Proceedings of the Symposium on the Application of Geophysics to Engineering and Environmental Problems (SAGEEP 1999), Oakland, Calif., March 14-18, p. 179-187.

Miller, R.D., D.W. Steeples, and M. Brannan, 1989, Mapping a bedrock surface under dry alluvium with shallow seismic reflections: *Geophysics*, v. 54, p. 1528-1534.

Miller, R.D., D.W. Steeples, and P.B. Myers, 1990, Shallow seismic-reflection survey across the Meers fault, Oklahoma: *GSA Bulletin*, v. 102, p. 18-25.

Miller, R.D., and D.W. Steeples, 1991, Detecting voids in a 0.6-m coal seam, 7 m deep, using seismic reflection: *Geoexploration*, Elsevier Science Publishers B.V., Amsterdam, The Netherlands, v. 28, p. 109-119.

Miller, R.D., N.L. Anderson, H.R. Feldman, and E.K. Franseen, 1995, Vertical resolution of a seismic survey in stratigraphic sequences less than 100 m deep in Southeastern Kansas: *Geophysics*, v. 60, p. 423-430.

Miller, R.D., J. Xia, C.B. Park, and J.M. Ivanov, 1999, Multichannel analysis of surface waves to map bedrock: *Leading Edge*, v. 18, n. 12, p. 1392-1396.

Miller, R.D., T.S. Anderson, J.C. Davis, D.W. Steeples, and M.L. Moran, 2001, 3-D characterization of seismic properties at the Smart Weapons Test Range, YPG: Proceedings of the Military Sensing Symposium on Battlefield Seismic and Acoustic Sensing, October 23-25, Laurel, Maryland, Published on CD.

Mooney, H.M., 1981, Handbook of engineering geophysics: Bison Instruments, Inc.

Nazarian, S., K.H. Stokoe II, and W.R. Hudson, 1983, Use of spectral analysis of surface waves method for determination of moduli and thicknesses of pavement systems: Transportation Research Record No. 930, p. 38-45.

Palmer, D., 1981, An introduction to the generalized reciprocal method of seismic refraction interpretation: *Geophysics*, v. 46, p. 1508-1518.

Park, C.B., R.D. Miller, and J. Ivanov, 2002, Filtering Surface Waves: Proceedings of the Symposium on the Application of Geophysics to Engineering and Environmental Problems (SAGEEP 2002), Las Vegas, Nevada, February 10-14, 2002.

Park, C.B., R.D. Miller, D.W. Steeples, and R.A. Black, 1996, Swept impact seismic technique (SIST): *Geophysics*, v. 61, p. 1789-1803.

Park, C.B., R.D. Miller, and J. Xia, 1999, Multichannel analysis of surface waves (MASW): *Geophysics*, v. 64, p.800-808.

Peterson, J.E., B.N.P. Paulsson, and T.A. McEvilly, 1985, Applications of algebraic reconstruction techniques to cross-hole data: *Geophysics*, v. 53, p. 1284-1294.

Pullan, S.E., and J.A. Hunter, 1990, Delineation of buried bedrock valleys using the optimum offset shallow seismic reflection technique: Soc. Explor. Geophys. Investigations in Geophysics no. 5, S.H. Ward, ed., *Volume 3: Geotechnical*, p. 75-87.

Redpath, B.B., 1973, Seismic refraction exploration for engineering site investigations, NTIS AD-768710.

Sander, J.E., 1978, The blind zone in seismic ground-water exploration: *Ground Water*, v. 165, p. 394-397.
Schepers, R., 1975, A seismic reflection method for solving engineering problems: *Journal of Geophysics*, v. 41, p. 267-284.
Scott, J.H., 1973, Seismic refraction modeling by computer, *Geophysics*, v. 38, p. 271-284.
Scott, J.H., 1977, SIPT–A seismic refraction inverse modeling program for timeshare terminal computer systems: U.S. Geological Survey Open-file Report 77-365.
Sheriff, R.E., 2002, *Encyclopedic Dictionary of Applied Geophysics*, 4th ed.: Tulsa, Society of Exploration Geophysicists, 429 p.
Shtivelman, V., U. Frieslander, E. Zilberman, and R. Amit, 1998, Mapping shallow faults at the Evrona playa site using high-resolution reflection method: *Geophysics*, v. 63, p. 1257-1264.
Soske, J.L., 1954, The blind zone problem in engineering geophysics: *Geophysics*, v. 24, p. 359-365.
Steeples, D.W., and R.D. Miller, 1990, Seismic reflection methods applied to engineering, environmental, and groundwater problems: Soc. Explor. Geophys. Investigations in Geophysics no. 5, S.H. Ward, ed., *Volume 1: Review and Tutorial*, p. 1-30.
Steeples, D.W., C.M. Schmeissner, and B.K. Macy, 1995, The evolution of shallow seismic methods: *Journal of Environmental and Engineering Geophysics*, v. 0, n. 1, p. 15-24 (invited paper).
Steinhart, J.S., and R.P. Meyer, 1961, Explosion studies of continental structure: Carnegie Institution of Washington Publication 622.
Stokoe II, K.H., S.G. Wright, J.A. Bay, and J.M. Roësset, 1994, Characterization of geotechnical sites by SASW method: in *Geophysical Characterization of Sites*, ISSMFE Technical Committee #10, ed. R.D. Woods, Oxford Publishers, New Delhi.
Telford, W.M., L.P. Geldart, and R.E. Sheriff, 1990, *Applied Geophysics*: Cambridge University Press, New York.
Tikhonov, A.N., and V.Y. Arsenin, 1977, *Solutions of Ill-posed Problems*: John Wiley and Sons.
Waters, K.H., 1987, *Reflection Seismology—A Tool for Energy Resource Exploration*, 3rd ed.: John Wiley and Sons, New York, 538 p.
Western Digital Climate Center, 2007, Monthly Total Precipitation, State University, New Mexico, http://www.wrcc.dri.edu/cgi-bin/cliMAIN.pl?nm8535, accessed May 10, 2007.
Xia, J., C. Chen, G. Tian, R.D. Miller, and J. Ivanov, 2005, Resolution of high-frequency Rayleigh-wave data: *Journal of Environmental and Engineering Geophysics*, v. 10, p. 99-110.
Xia, J., R.D. Miller, C.B. Park, J.A. Hunter, J.B. Harris, and J. Ivanov, 2002, Comparing shear-wave velocity profiles from multichannel analysis of surface wave with borehole measurements: *Soil Dynamics and Earthquake Engineering*, v. 22, n. 3, p. 181-190.
Xia, J., R.D. Miller, and C.B. Park, 1999, Estimation of near-surface velocity by inversion of Rayleigh waves: *Geophysics*, v. 64, p. 691-700.
Yilmaz, O., 1987, *Seismic Data Processing*; S.M. Doherty, ed.; in Series: Investigations in Geophysics, no. 2, E.B. Neitzel, series ed.: Soc. Explor. Geophys.
Zhang, J., and M.N. Toksoz, 1998, Nonlinear refraction traveltime tomography: *Geophysics*, v. 63, p. 1726-1737.